

SPOKESMAN - H.L. ANDERSON  
ENRICO FERMI INSTITUTE  
UNIVERSITY OF CHICAGO  
CHICAGO, ILLINOIS 60637  
TELEPHONE - (312) 753-8713

TEVATRON PROPOSAL  
FOR A STUDY OF  
ELECTROWEAK INTERFERENCE  
IN  
DEEP INELASTIC MUON SCATTERING  
AT  
600 and 750 GeV

PARTICIPATING PHYSICISTS

UNIVERSITY OF CHICAGO

S.C. Wright

LOS ALAMOS SCIENTIFIC LABORATORY

H.L. Anderson, W.W. Kinnison, R.J. McKee, S. Wipf

NATIONAL RESEARCH COUNCIL, CANADA

C.K. Hargrove

UNIVERSITY OF OXFORD

W.S.C. Williams

April 24, 1980

62 pgs.

ELECTROWEAK INTERFERENCE IN DEEP INELASTIC MUON SCATTERING  
AT 600 AND 750 GeV

UNIVERSITY OF CHICAGO

S.C. Wright

LOS ALAMOS SCIENTIFIC LABORATORY

H.L. Anderson, W.W. Kinnison, R.J. McKee, S. Wipf

NATIONAL RESEARCH COUNCIL, CANADA

C.K. Hargrove

UNIVERSITY OF OXFORD

W.S.C. Williams

SUMMARY

The electroweak interference in deep inelastic muon scattering will be studied in a superconducting air gap spectrometer using gated time projection chambers for precise measurement of the momenta of the incident and scattered muons and the angle between them. The geometric acceptance will be close to 100%. A total of 4400 hours of good muon beam is required. This includes both  $\mu^+$  and  $\mu^-$  at two energies,  $E_\mu = 750$  and 600 GeV. The experiment contemplates 1 year for setting up and tuning, 2 years of running beginning January 1985. The experiment is a high  $Q^2$  test of the Weinberg-Salam model and a measurement of the Weinberg angle with an uncertainty of  $\delta \sin^2 \theta_w = 0.010$ .

SPOKESMAN - H.L. ANDERSON  
ENRICO FERMI INSTITUTE  
UNIVERSITY OF CHICAGO  
CHICAGO, ILLINOIS 60637  
TELEPHONE - (312) 753-8713

April 24, 1980

## Deep Inelastic Muon Scattering at 600 and 750 GeV

### Abstract

We propose to study deep inelastic muon scattering at 600 and 750 GeV using a superconducting air gap magnet spectrometer. Our spectrometer accommodates a long target with close to 100% acceptance and high resolution over most of the kinematic range. The spectrometer is versatile and could be used to study many aspects of deep inelastic scattering. Here, however, we describe in detail a proposal to measure the electroweak interference effect as a high  $Q^2$  test of the Weinberg-Salam model and as a measurement of the Weinberg angle.

## 1. Introduction

At the Tevatron the 750 GeV muon beam will have about 3 times the energy of the beams that have been available at Fermilab and CERN. This has the advantage of extending the kinematic range into the region where the uncertainties and ambiguities of an interpretation of the data based on Quantum Chromodynamics will be less serious than in the work to date. Thus, the deviations from lowest order QCD seen in the Fermilab  $\mu p$  and  $\mu d$  experiments and ascribed to higher order corrections, should be much less at 750 GeV. However, at 750 GeV new effects can be expected which will complicate an analysis of the data based on QCD alone. We mention the electroweak interference, two photon exchange, and new quark thresholds among others. These effects need to be identified and isolated before a QCD analysis can properly proceed, but they have an interest in their own right. In fact, the prospect of carrying out a measurement of the electroweak interference effect at high  $Q^2$  has captured our imagination. We believe that the idea of unification is of transcendent importance in physics and that an opportunity to add to its experimental underpinning should be pursued with utmost vigor. We are submitting this proposal with that in mind.

## 2. Electroweak Interference

The electroweak interference effect is a necessary consequence of any theory which unifies the weak and the electromagnetic interactions. Persuasive evidence for this effect was provided by the Prescott <sup>(1)</sup> experiment. This experiment compared the inelastic scattering of right

and left handed polarized electrons from an unpolarized deuterium target. They found an asymmetry in the inclusive cross-sections  $A = (\sigma_R - \sigma_L)/(\sigma_R + \sigma_L) = (-9.5 + 1.6) \times 10^{-5} Q^2$ ,  $Q^2$  in  $(\text{GeV}/c)^2$ , for values of  $Q^2$  near 1.4. The experiment was in fine agreement with the Weinberg-Salam model. It catapulted this model into undisputed prominence and gave strong support to the idea that underlying the laws of nature there is a grand principle of unification. In nature the underlying symmetries are made mysterious and remain concealed by processes which break the symmetry, but Weinberg and Salam had found the common symmetry that joins the weak and the electromagnetic interactions and identified the symmetry breaking mechanism that makes them different in appearance.

In view of these considerations it seems important to carry out experimental tests of the Weinberg-Salam model at the highest values of  $Q^2$  available. The Prescott result already makes evident that at the Tevatron with  $Q^2 \approx 400 (\text{GeV}/c)^2$  the electroweak interference will be a 4% effect. The experiment we propose can measure the Weinberg parameter  $\sin^2\theta_W$  with an uncertainty  $\pm 0.01$ .

### 3. Muon Experiments

In Table I we list some of the standard experiments that are done with high energy muon beams. The added interest at  $E_\mu = 750 \text{ GeV}$  is because of the larger dynamic range available. This is shown in Figure 1 where  $Q^2$  and  $x$  are given in terms of the measured quantities  $\nu = E - E'$  and  $\theta$ . The higher order effects that plague tests of QCD at lower energies will be appreciably smaller at 750 GeV. Since QCD effects are small, it will be necessary to do the measurements with high precision.

For the electroweak interference experiment we propose to use a long Be target for the high luminosity this can give. To separate the effects of the neutron and proton and to determine the quark and gluon structure of the nucleon in appropriate detail liquid hydrogen and deuterium targets will be required in possible future work that we do not emphasize here.

Table 1

## Experiments with High Energy Muons\*

1. Electroweak interference
2. Double  $\gamma$  exchange
3.  $F_2(x, Q^2)$   $10 \leq Q^2 \leq 500 \text{ GeV}^2$   
See if  $F_2(x, Q)$  rises at low  $x$  and falls at high  $x$  with  $Q^2$
4. Measure  $R = \sigma_L / \sigma_T$
5. Better Moments  
$$M(n, Q^2) = \int x^{n-2} F_2(x, Q^2) dx$$
  
"Test QCD"
6. Check if  $M^N(n, Q^2) \rightarrow M^P(n, Q^2)$
7. Low  $x$  behavior; Quark thresholds
8. Multi-muons,  $J/\psi$ ,  $T$  production
9. Quark and Gluon Jets
10. Weak charged current processes
11. Surprises?

\* In terms of the measured quantities incident energy  $E$ , scattered energy  $E'$ , angle  $\theta$ , and the nucleon mass  $M$ , we use  $Q^2 = 4EE'\sin^2(\theta/2)$ ,  $\nu = E - E'$ ,  $x = Q^2/2M\nu$  and  $y = \nu/E$ .



Such measurements will need a spectrometer with the following characteristics:

- i) High acceptance, approaching 100% over most of the kinematic range.
- ii) Accommodation for a long target,  $\approx 50$  meters, for adequate statistics at large  $Q^2$ .
- iii) High resolution in angle and momentum.

Such performance can be obtained with a magnetic spectrometer having a 50 meter target inside the magnetic field and instrumented with an array of time projection chambers having a time resolution of 1 nano-second and a spatial resolution of 100 microns. The long target is needed because the large values of  $Q^2$  that we want to reach have low cross-sections. However, since scattering angles are small we can work with a magnet of small aspect ratio. Our magnet is very long, 60 meters, compared to 80 cm x 80 cm for the width and height of its useful magnetic field.

Such arrangements have been used before. The CERN muon scattering experiment NA-4 uses a 50 meter long liquid hydrogen target surrounded by a toroidal iron magnet. This spectrometer was specially designed to measure scattering at high  $Q^2$ . However, such iron magnets are not suitable if precision is important because multiple scattering in the iron limits the resolution obtainable in angle and momentum. This problem is aggravated for muon energies approaching the critical energy, 870 GeV in iron, because radiative losses in single collisions can be quite large and are difficult to correct for. For accurate work it is better to measure angles and momenta in an air gap magnet.

Another serious drawback in all previous spectrometers used for deep inelastic muon scattering is that their acceptance is appreciably less than 100% and varies with the scattering angle and energy in such a complex way that the correction must be done using the Monte Carlo method. Without an enormous amount of computing there will always be uncertainties in this acceptance correction over the whole  $Q^2, \nu$  plot. It is because of this that it is a great advantage to keep the acceptance near 100% and the corrections small.

#### 4. Quark Distributions

Our calculations are based on quark momentum distributions obtained by extrapolating a Buras and Gaemers <sup>(2)</sup> type fit of current muon, electron, and neutrino scattering data in the range  $2 \leq Q^2 \leq 200 \text{ GeV}^2$  to  $Q^2 = 1500 \text{ GeV}^2$ . Figure 2 shows the quark momentum distributions at 50 and 500  $\text{GeV}^2$ . The calculations were made in leading order QCD without allowance for higher order effects or for quark flavors beyond charm.

Figure 3 shows the structure function  $F_2(x, Q^2)$  per nucleon for the deuteron (average of proton and neutron) up to  $Q^2 = 1,000 \text{ GeV}^2$ , obtained from the extrapolated quark distributions. These were adjusted to fit the data at low  $Q^2$  without taking higher order effects into account. The extrapolation to high  $Q^2$  were made without taking into account higher order effects either. The measurements at high  $Q^2$  offer's the prospect of showing how much these effects amount to.

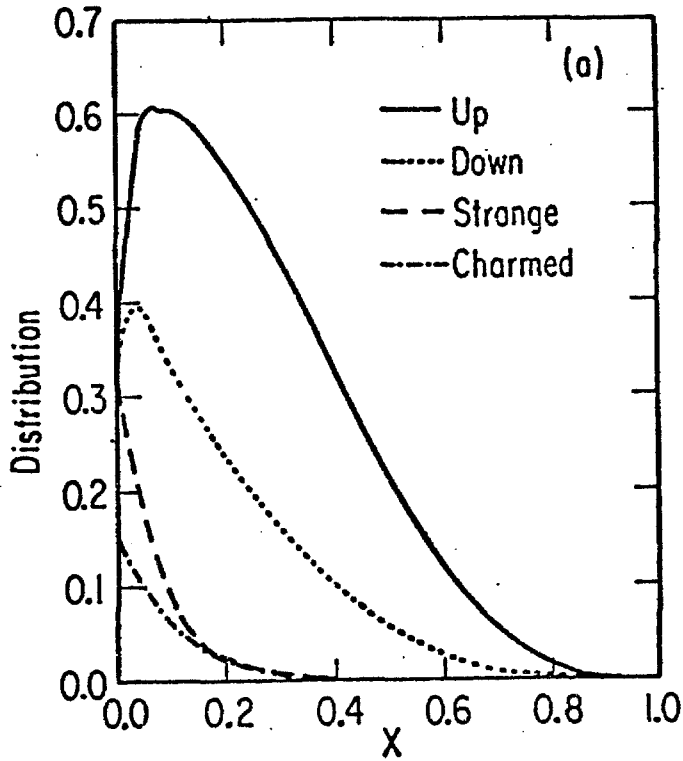


Figure 2a

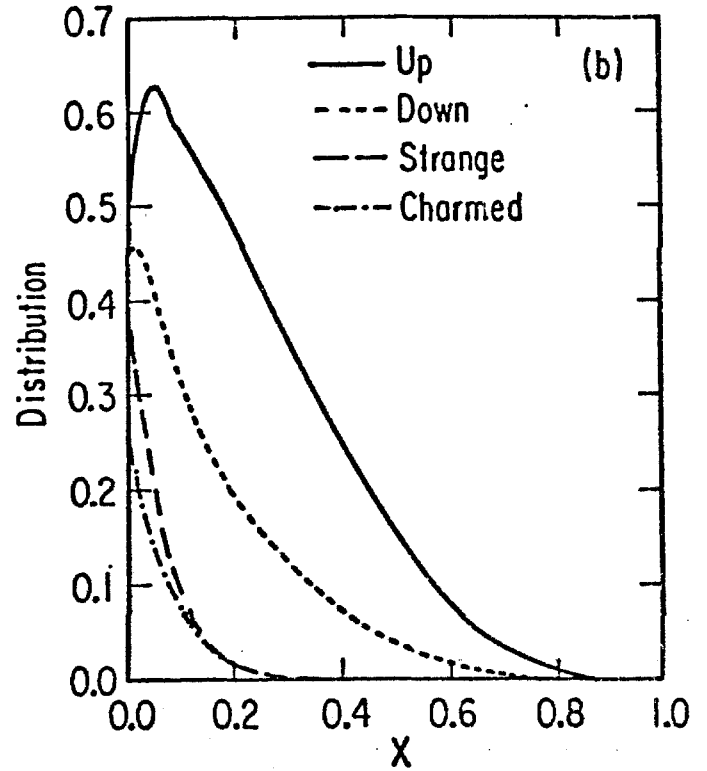


Figure 2b

Figure 2: Quark momentum density distributions at (a)  $Q^2 = 50 \text{ GeV}^2$ , (b)  $Q^2 = 500 \text{ GeV}^2$ , as deduced from a fit of the current set of structure function measurements from SLAC, Fermilab and CERN, including the CDHS neutrino data. We used the procedure of Buras and Gaemers in obtaining a set of quark and gluon distribution functions which satisfy QCD and fit the data. As  $Q^2$  is increased the momentum densities rise at small  $x$ , fall at large  $x$ , but the changes over all are not large.

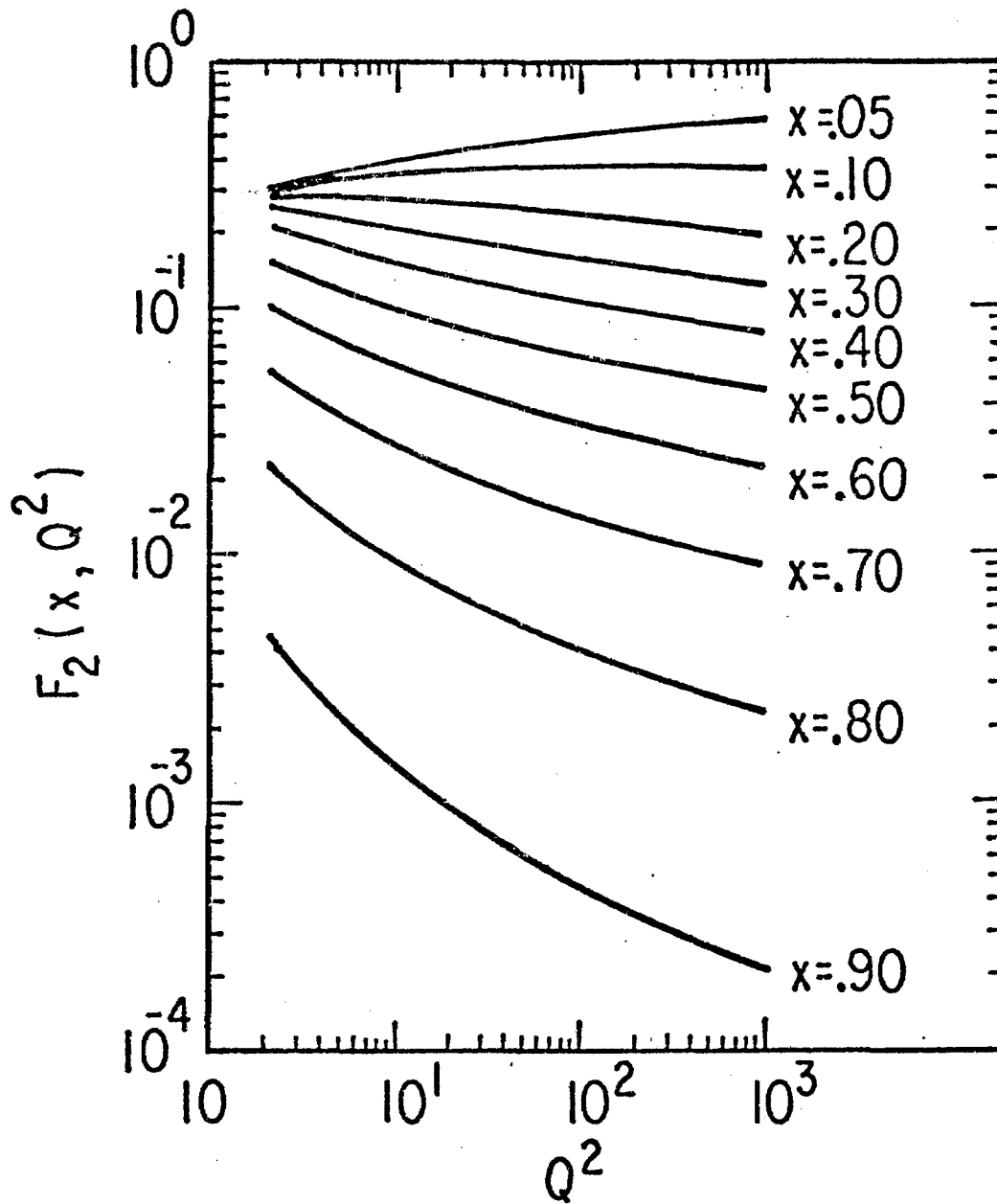


Figure 3: The structure function  $F_2(x, Q^2)$  per nucleon for deuterium for various values of  $Q^2$  up to  $Q^2 = 1000 \text{ GeV}^2$  using the Buras and Gaemers method to extrapolate the fit made with the data in the range  $2 \leq Q^2 \leq 200 \text{ GeV}^2$ .

## 5. Effect of Resolution

Figure 4 is shown to emphasize the importance of high acceptance and high resolution in the measurement. The cross-section has a steep dependence on both energy and angle. The numbers of events shown in the figure have been calculated for an integrated luminosity of  $10^{40}$   $\mu$ 's x nucleons/cm<sup>2</sup> by integrating over bins with  $\Delta x = \Delta y = 0.2$ . If the cross-sections were flat the result would be insensitive to the shape and width of the resolution function. However, in our case the dependence is very steep and a precise knowledge of the resolution function and the acceptance is required to take proper account of the overpopulation of events of small angle and low energy in the bin. The width of the resolution function brings such events into the bin in greater number than it takes away. As indicated in the figure the fractional uncertainty in measuring the cross-section near  $y = 0.5$  is about 10 times the fractional uncertainty in measuring the scattering angle. Even if the acceptance and resolution function were precisely known and properly accounted for there would still be a reduction in statistical accuracy because of the way the events are redistributed over the bins.

## 6. Ratio of $\mu^-$ and $\mu^+$ Cross-Sections

High energy muons in the usual muon beam come from pions (and kaons) decaying in the forward direction. As a consequence the  $\mu^-$  beam is predominantly longitudinally polarized in the unnatural sense, right handed. The  $\mu^+$  beam is polarized predominantly left handed. At  $E_\mu = 750$  GeV the polarization estimated from the energy distribution <sup>(3)</sup>

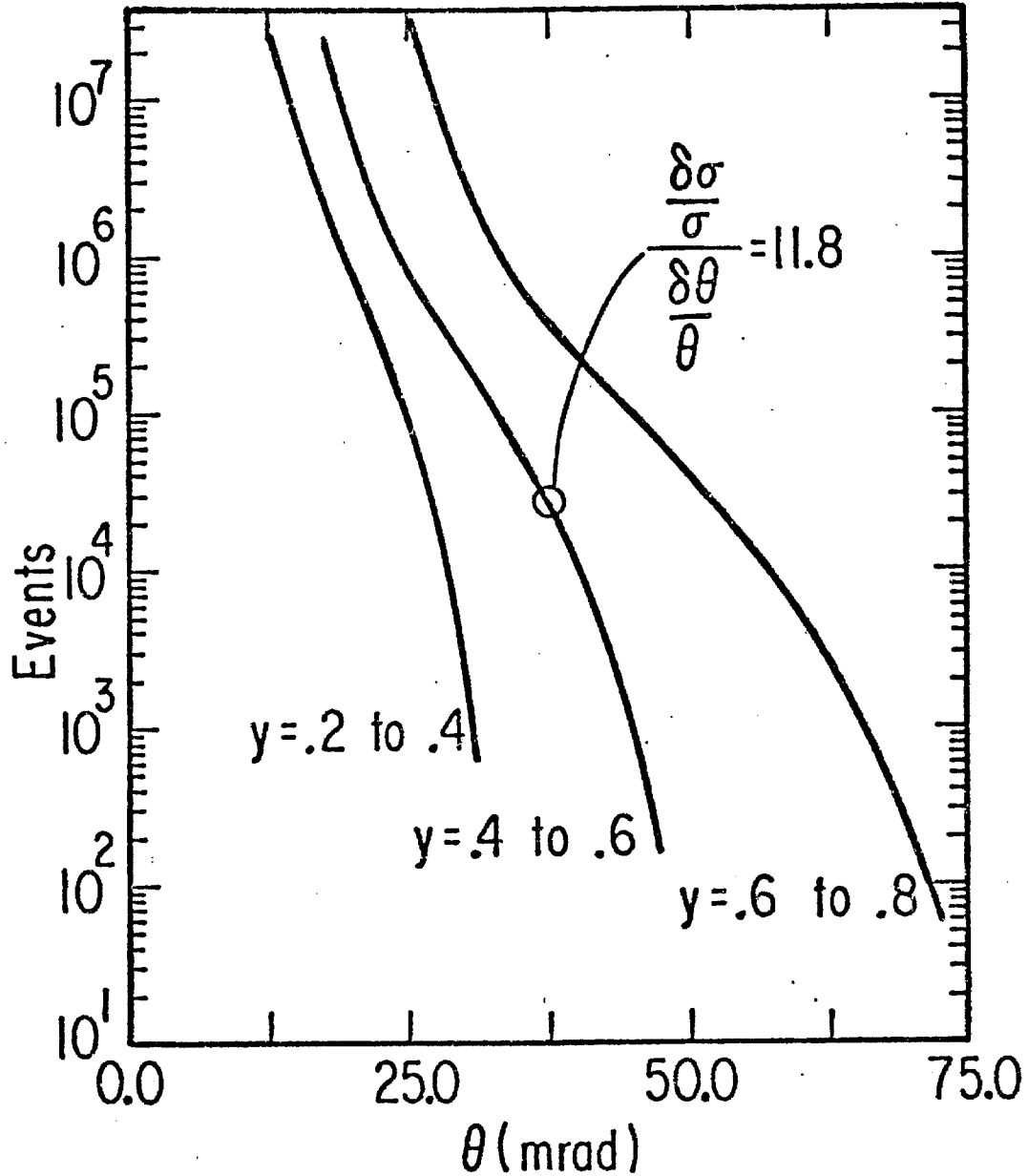


**Figure 4:** Counting rates expected at  $E_{\mu} = 750$  GeV as a function of scattering angle for various values of  $y = \nu/E$ . The rates are calculated for bins with  $\Delta x = 0.2$ ,  $\Delta y = 0.2$  and total luminosity  $10^{40}$  muons x nucleons/cm<sup>2</sup>. The steep dependence of the scattering angle emphasizes the importance of precise measurement of the scattering angle. At the circled point the fractional error in the cross-section we want to measure is 12 times the uncertainty in the measurement of the scattering angle.

of the parent pions is close to 90%. The polarization is only slightly less for  $E_\mu = 600$  GeV. In view of this the most straightforward way to study the electroweak interference is to compare the inclusive cross-sections for  $\mu^+$  and  $\mu^-$  scattering over a suitably chosen kinematic range. Additional information can come from a Prescott type experiment in which the opposite polarizations of the same sign muon are compared, but high energy muon beams polarized in the natural sense are more difficult to come by and would have lower energy and lower intensity. We do not propose to use such beams here.

Figure 5 shows the ratio of the single photon exchange cross-section with and without the electroweak effect, calculated<sup>(4)</sup> using the Weinberg-Salam model with  $\sin^2\theta_w = 0.21$ . The ratios are for right and left handed  $\mu^+$  and  $\mu^-$  beams at  $E_\mu = 750$  GeV. The electroweak interference effect increases the single photon exchange cross-section for  $\mu^-$ , and decreases it for  $\mu^+$ .

The effect can be as large as 30% in the  $\mu^-$  case, 20% in the  $\mu^+$  case. However, these values occur for large values of  $x$  and  $y$  for which the counting rates will be impractically small. In a practical experiment most of the events will be at smaller values of  $x$  and  $y$  where the smaller effect is compensated by better statistical accuracy.

## 7. Rates

We have estimated the rates to be expected and the accuracy obtainable in a practical experiment measuring the ratio of the inclusive cross-sections for  $\mu^-$  and  $\mu^+$  on a Be target. The estimates are for a total integrated

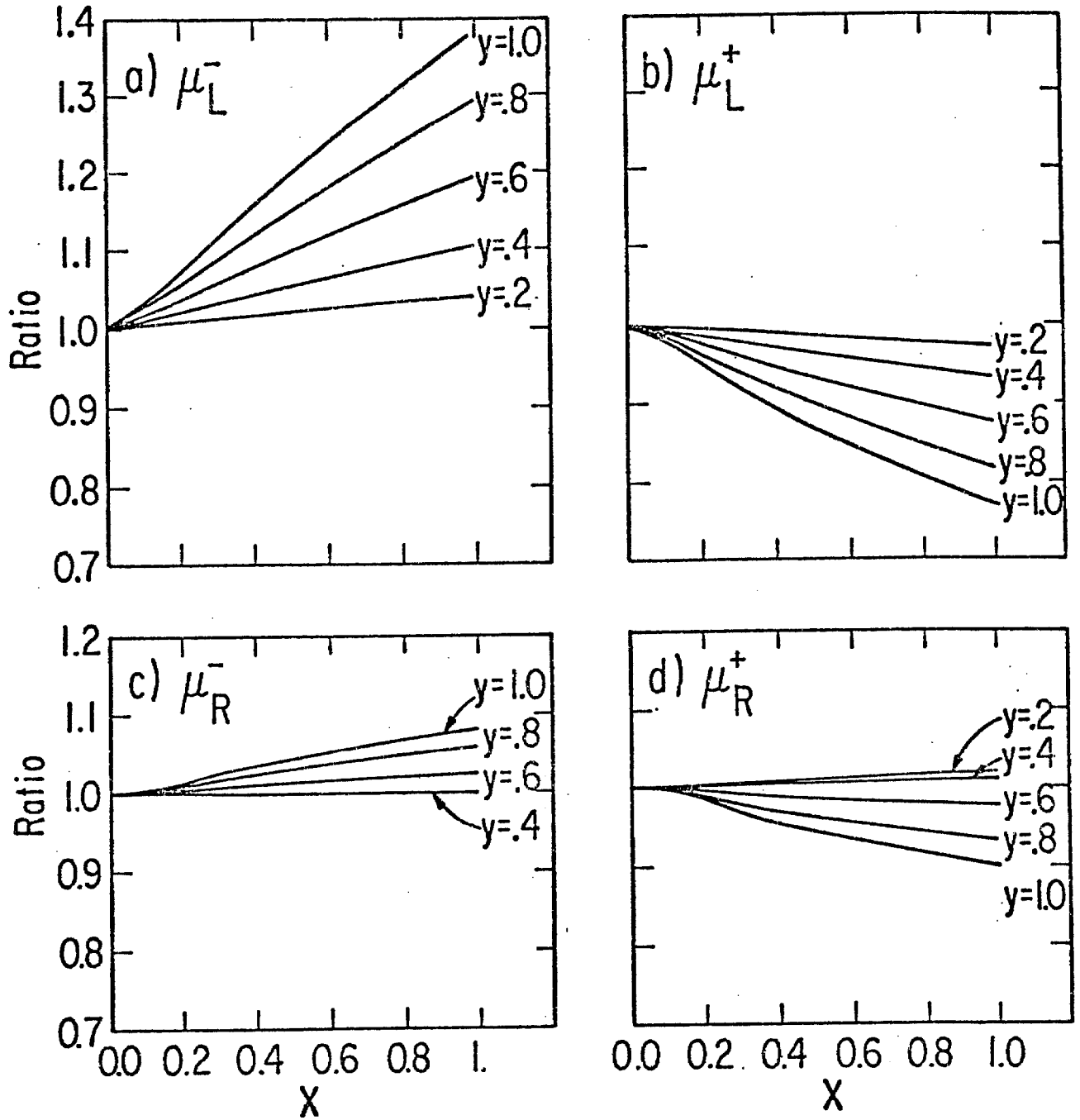


Figure 5: Plots of the total to 1 photon exchange cross-section ratio for  $\mu^-$  and  $\mu^+$  with right and left handed polarization for  $E_\mu = 750$  GeV on an isoscalar target. The calculation is based on the Weinberg-Salam model with  $\sin^2\theta_W = 0.21$ . The effect can be quite large, more than 30% for  $\mu_L^-$ . Note  $\mu^-$  ratios are greater than 1,  $\mu^+$  less than 1. The  $\mu^-$  beam from forward decaying  $\pi^-$  is polarized 90%  $\mu_R^-$  + 10%  $\mu_L^-$ . For  $\mu^+$  the polarization mix is 90%  $\mu_L^+$  + 10%  $\mu_R^+$ .

luminosity of  $10^{40}$  muons x nucleons/cm<sup>2</sup>, obtainable by running with a beam of average intensity  $2 \times 10^6$  muons/sec for  $10^6$  seconds on a Be target 50 meters long. The rates refer to a spectrometer with 100% acceptance and 100% detection efficiency. The calculations were based on the Weinberg-Salam model under the following conditions:

- 1a)  $E_\mu = 750$  GeV,            1b)  $E_\mu = 600$  GeV
- 2)  $\sin^2\theta_W = 0.21$
- 3)  $E'_\mu > 100$  GeV
- 4)  $10 < \theta_{\text{scatt}} < 120$  mrad
- 5) Longitudinal polarization:
  - a)  $\mu^-$  90% left handed
  - b)  $\mu^+$  90% right handed
- 6) Integrated luminosity  $10^{40}$   $\mu$  x nucleons/cm<sup>2</sup>.

The ratios and their statistical errors in bins of  $\Delta x = \Delta y = 0.2$  are shown in Figures 6a and 6b for  $E_\mu = 750$  GeV and  $E_\mu = 600$  GeV respectively. The statistical accuracy in the measurement of the Weinberg parameter is  $\delta\sin^2\theta_W = 0.008$  and  $0.009$  for the 750 and 600 GeV experiments, respectively. Not much is lost in statistical accuracy if the angular range is restricted somewhat. In Table 2 we list the number of events expected in the angular range  $20 \leq \theta \leq 70$  mrad. In this case  $\delta\sin^2\theta_W = 0.0092$  at  $E_\mu = 750$  GeV. Over this more limited angular range the angles can be measured with more accuracy and greater redundancy. The trigger requirement can be tightened and the number of background events made smaller.

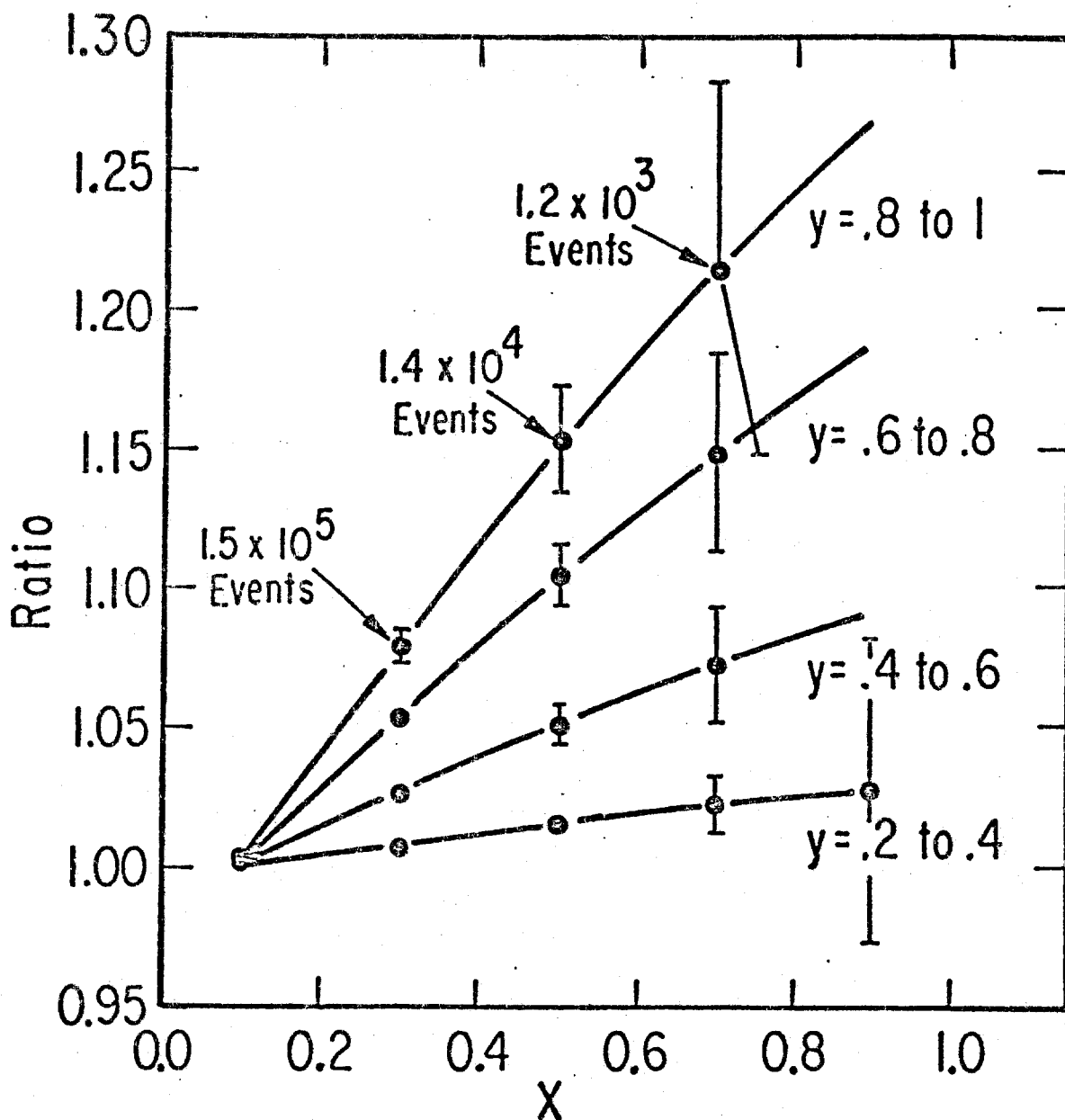


Figure 6a: Expected ratio of counts in bins with  $\Delta x = 0.2$ ,  $\Delta y = 0.2$  for  $\mu^+$  and  $\mu^-$  based on the Weinberg-Salam model,  $\sin^2\theta_w = 0.21$ . The integrated luminosity is  $10^{40}$  muons x nucleons/cm<sup>2</sup> at  $E_\mu = 750$  GeV. An indication of the total number of events ( $\mu^+ + \mu^-$ ) expected is indicated for the curve  $y = 0.8$  to  $1.0$ . These range from  $1.5 \times 10^5$  events at  $x = 0.3$  to 290 events at  $x = 0.9$ . The point at  $x = 0.1$  is a high statistics point which should show little asymmetry and will be used as a check against systematic errors. Radiative corrections and the effect of 2 photon exchange are not included in this calculation. The Weinberg angle can be determined to an uncertainty  $\delta\sin^2\theta_w = 0.008$  (statistical).

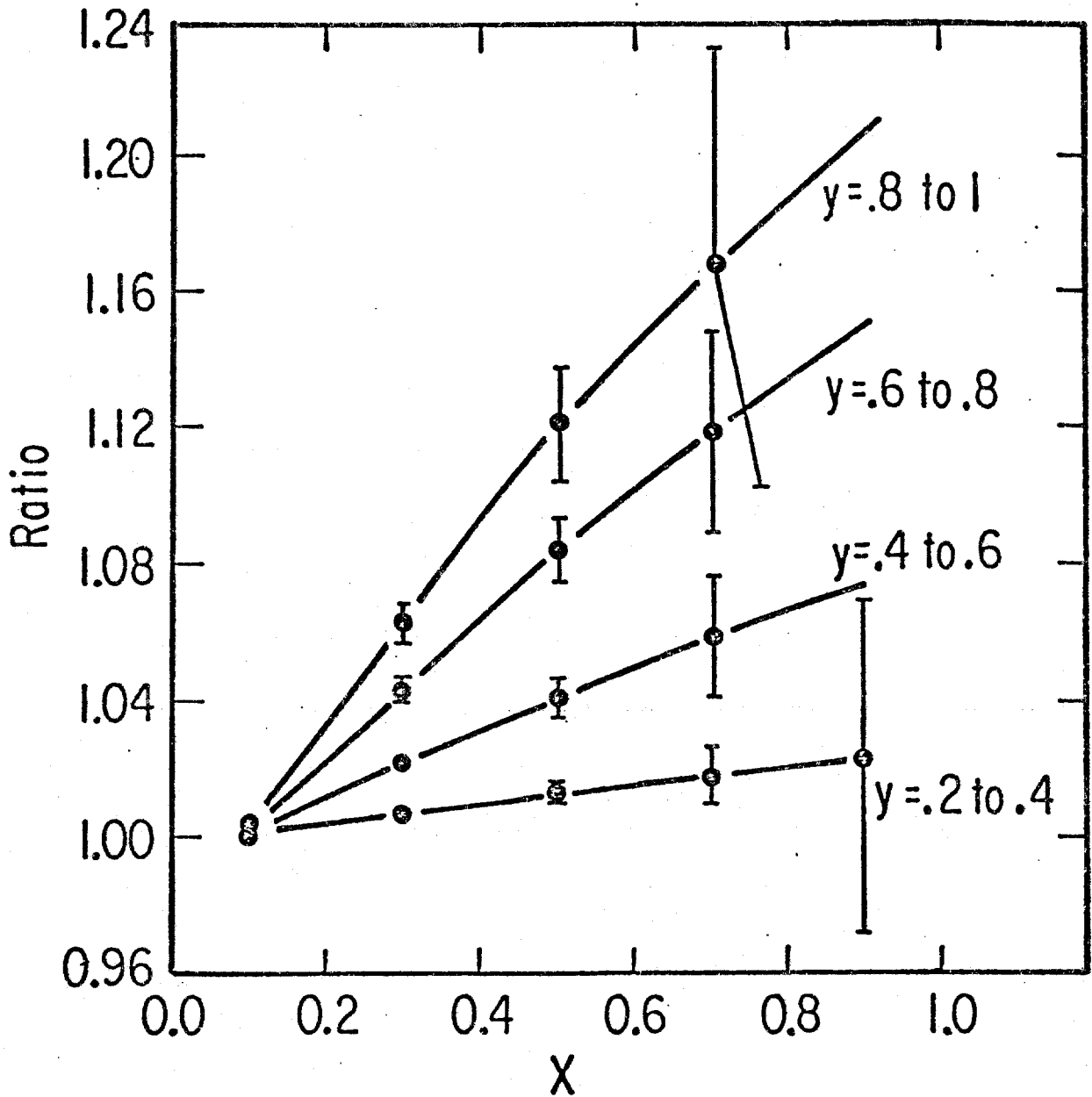


Figure 6b: Ratio  $\mu^-$  to  $\mu^+$  events at  $E_\mu = 600$  GeV. The Weinberg angle is determined to an accuracy of  $\delta\sin^2\theta_W = 0.009$  (statistical). The effect is smaller at 600 GeV but the cross-section is larger. A check on 2 photon exchange effects can be obtained by studying the  $Q^2$  dependence as a function of  $E_\mu$ .

TABLE 2

Expected number of events for an integrated luminosity of  $10^{40}$  muons x nucleons/cm<sup>2</sup> at  $E_\mu = 750$  GeV. Calculated with polarizations 90%  $\mu_L^+$ , 90%  $\mu_R^-$  for  $\sin^2\theta_W = 0.21$ ,  $E'_\mu \geq 100$  GeV,  $20 \leq \theta_{\text{scatt}} \leq 70$  mrad.

	$\theta_{\text{min}}$	$\theta_{\text{max}}$	Events		Ratio* ( $\mu^-/\mu^+$ )
			$\mu^+$	$\mu^-$	
y=0.2-0.4		mrad			
x					
0.2-0.4	20.0	25.8	119880	122130	1.0188 (45)
0.4-0.6	20.0	31.6	104040	106230	1.023 (10)
0.6-0.8	20.0	36.5	20320	20785	1.023 (10)
0.8-1.0	22.4	40.8	693	712	1.028 (55)
y=0.4-0.6					
x					
0.0-0.2	20.0	27.4	311910	317030	1.0164 (26)
0.2-0.4	20.0	38.7	378360	388930	1.0279 (23)
0.4-0.6	25.8	47.5	48248	50747	1.0518 (67)
0.6-0.8	31.6	54.8	5035	5403	1.073 (21)
0.8-1.0	36.5	61.3	157	172	1.09 (12)
y=0.6-0.8					
x					
0.0-0.2	20.0	44.7	1493000	1513100	1.0134 (12)
0.2-0.4	27.4	63.3	168880	178040	1.0542 (36)
0.4-0.6	38.7	70.0	19051	21036	1.104 (11)
0.6-0.8	47.5	70.0	1592	1814	1.140 (39)
0.8-1.0	54.8	70.0	36	42	1.17 (26)
y=0.8-1.0					
x					
0.0-0.2	20.0	57.0	1213000	1223700	1.0088 (13)
0.2-0.4	44.7	70.0	36073	38717	1.0733 (79)
0.4-0.6	63.3	70.0	809	912	1.128 (54)

\*Statistical error in the last figure in parenthesis ( ).

## 8. Superconducting Magnet Spectrometer

A cross-section through the spectrometer magnet is shown in Figure 7. The iron yoke is from the Cosmotron magnet and is 2.4m across the flats. The useful aperture is 80 cm x 80 cm and the magnet can operate up to 20,000 gauss with a highly uniform magnetic field. The superconducting coils are inside a 15 cm thick cryostat jacket. A space allowance of 10 cm top and bottom is provided for the time projection chamber wires and readout. A beryllium target 10 cm x 10 cm is shown as it would be used for the electroweak interference experiment. This would be replaced by liquid hydrogen and liquid deuterium targets of 10 cm diameter for structure function determinations.

Figure 8 shows a longitudinal view of the spectrometer. There are 10 magnet modules each 6 meters long. The Be target runs through the first 8 magnets. The remaining two magnets at the far end are used to allow sufficient measuring space for the events that occur in the downstream portion of the target. The iron yoke serves as a muon identifier and is equipped with scintillation counters and drift chambers. The scintillation counters produce a trigger for muons that have penetrated an appreciable thickness of iron and are moving outward in the iron; the drift chambers point the scattered muon back to the vertex.

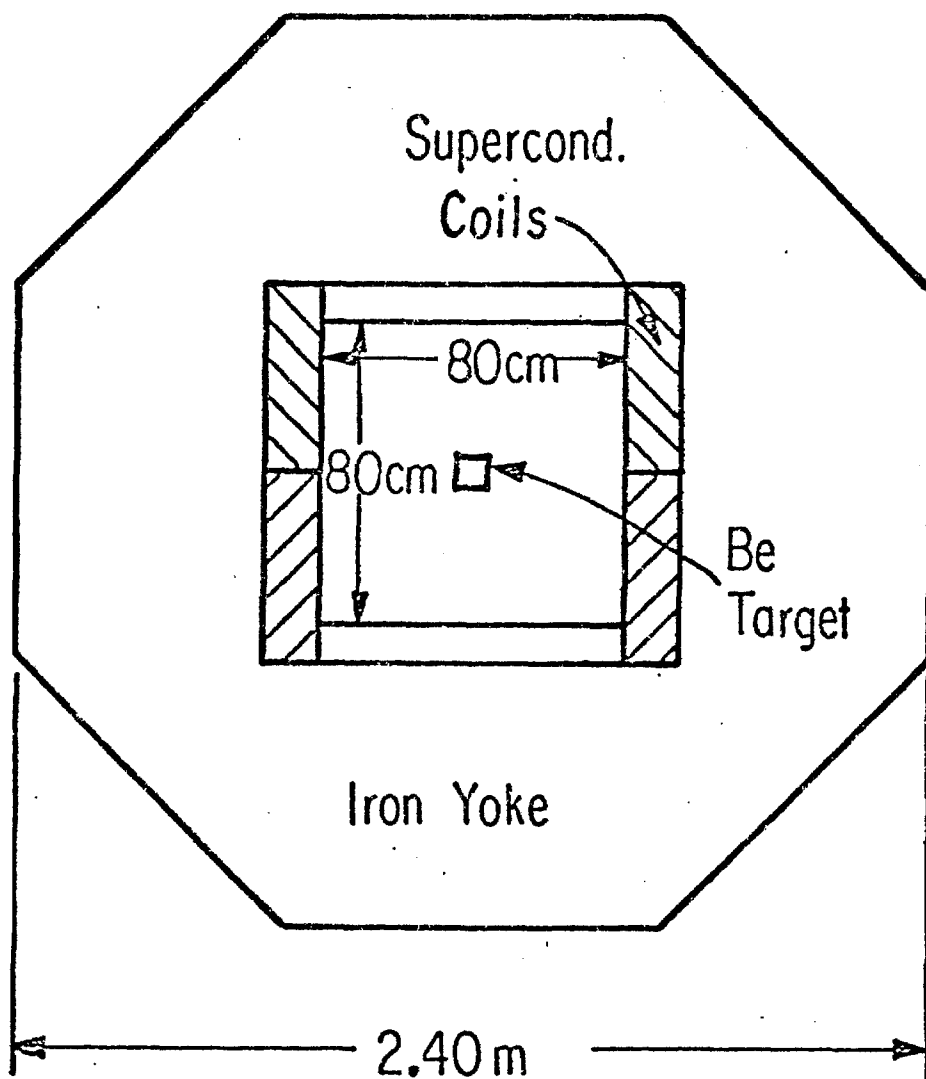


**Figure 7:** Cross-section through the superconducting air gap spectrometer. The iron yoke is from the Cosmotron magnet, 2.4 m across the flats. The useful aperture is 80 cm x 80 cm and has a highly uniform 20,000 gauss field. The superconducting coils are inside a 15 cm thick cryostat jacket; 10 cm top and bottom are for the time projection chamber readouts. A beryllium target will be used for the electro-weak interference experiment.

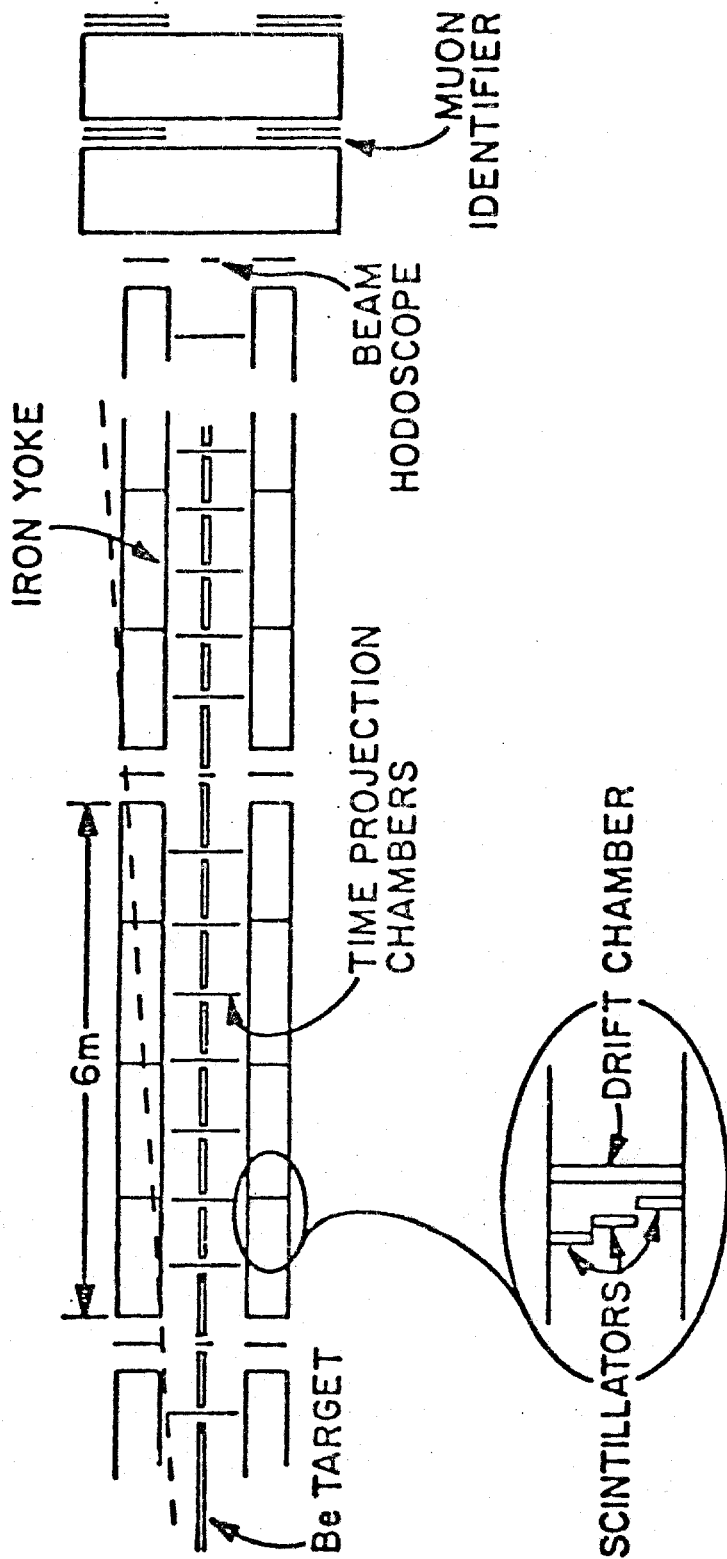


Figure 8: Longitudinal view of superconducting air gap spectrometer. There are 10 magnet modules each 6 meters long. The Be target used for the electron-weak interference experiment runs through the first 8 magnets. Two additional magnets at the far end are used to measure the muons from the downstream end of the target. The iron yoke serves as a muon identifier and is equipped with scintillation counters and drift chambers. The scintillation counters produce a trigger for muons that have penetrated an appreciable thickness of iron and are moving outward in the iron; the drift chambers point the scattered muon back to the vertex. Precision measurements of momentum and angle are obtained with time projection chambers that operate in the 20,000 gauss magnetic field. The muon identifier at the end is for small angle scattered muons which have not penetrated the magnet yoke sufficiently.

Precision measurements of momentum and angle are obtained with time projection chambers that operate in the 20,000 gauss magnetic field. The muon identifier at the end is for small angle scattered muons which have not penetrated a sufficient length of magnetic yoke. More detail on the design of the superconducting magnet is given in Appendix A.

#### 9. Flash Encoder Readout

The flash encoder makes possible 1 ns time resolution and 100  $\mu\text{m}$  space resolution obtainable with the time projection chamber. The flash encoder (TRW model number TDC1007J) is an 8 bit fully parallel analog to digital converter capable of digitizing an analog signal every 40 ns. It has 255 sampling comparators, and if this is followed by a 512 step 8 bit shift register, 20 microseconds of pulse height data can be stored and then read out to a computer if desired.

The sketch in Figure 9a indicates how an electron avalanche at the sense wire induces charge among a series of pads. The flash encoder records the shape of each pulse by digitizing the height of a sample every 40 nanoseconds as indicated in Figure 9b.

The 1st moment of the time distribution can be obtained to a fraction of 40 nanoseconds, or about 1 nanosecond. The space resolution is obtained from the 1st moment of the charge induced in an array of pads underneath the sense wire. We use one flash encoder for each pad and integrate the 40 nanosecond samples to get the total charge induced on each pad. With 8 bit digitizers it should be possible to interpolate between pads to an accuracy of 1% of the 1 cm spacing, or 100  $\mu\text{m}$ .

For precise timing we use a pair of time projection chambers as shown in Figure 9c, one with electrons drifting up from the track, the other with the drift down. The trigger provides the start time for the flash encoder clock. By measuring  $t_1$  and  $t_2$  for the up and down drifted electrons, we measure the location of the track  $y = (t_2 - t_1)/(t_1 + t_2)$  as a fraction of the total height above (or below) the median plane. Such a measurement is independent of the value of the drift velocity, provided only that it is the same for both chambers and uniform within them. Out-of-time tracks are readily recognized as having the wrong  $t_1 + t_2$ . Since the drift velocity in the argon-CH<sub>4</sub> gas mixture commonly used is 5 cm/μs, a 1 ns measurement corresponds to 50μm in  $y$ . With these accuracies we can obtain  $\Delta p/p \leq 2\%$ ,  $\Delta\theta/\theta \leq 0.1\%$  over the range of momentum and angle of interest here.

#### 10. Time Projection Chamber

The simple time projection chamber we describe can handle a reasonably high multiplicity of tracks. To the extent that the tracks in a shower are distributed in  $y$  and  $x$  they will be read out sequentially in time at the different pads as the electrons they produce arrive at the sense wire. The measurement of  $x$  requires the pulse height information of 3 pads over a region  $\Delta x \approx 3\text{cm}$ . The measurement of  $y$  uses the time information over the duration of the pulse  $\approx 120\text{ ns}$  or  $\Delta y \approx 0.6\text{cm}$ . Thus, two particles in a shower can be resolved if they are separated by either 3cm in  $x$  or 0.6 cm in  $y$ .

In general, it will be easy to identify the track of the scattered muon with little confusion from the hadronic shower that accompanies the scattering. This is because the hadrons are emitted with small transverse

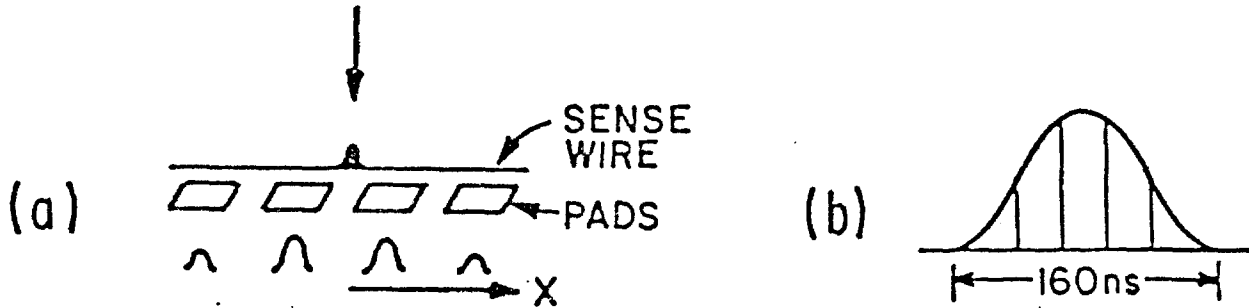


Figure 9: The Flash Encoder Readout. The flash encoder readout makes possible 1 ns time resolution and  $100\mu\text{m}$  space resolution with the time projection chamber. (b) The flash encoder records the shape of a pulse by digitizing the pulse height of a sample of the pulse every 40 nanoseconds and storing this information in a shift register. The first moment of the time distribution can be obtained to a fraction of 40 nanoseconds, or about 1 nanosecond. (a) The space resolution is obtained from the first moment of the samples of charge induced in the cluster of pads underneath the sense wire of the time projection chamber. We use one flash encoder for each pad and integrate the 40 nanosecond samples to get the total charge induced in each pad.

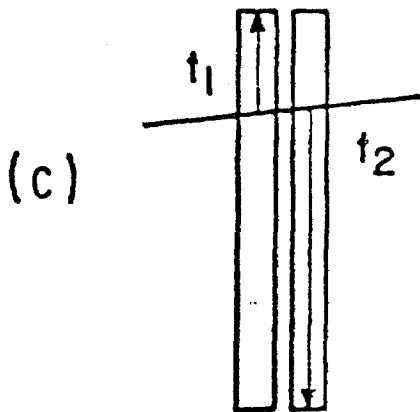


Figure 9c: For precise timing we use a pair of time projection chambers, one with electrons drifting up, the other with drift down. The trigger provides the start time for the flash encoder clock. By measuring  $t_1$  and  $t_2$  for up and down drifted electrons we measure the location of the track in the y direction and also the drift velocity in the chamber. Tracks that are out of time with the trigger will give a wrong  $t_1 + t_2$ . The ratio difference over sum gives the position independent of the drift velocity. Since the drift velocity in Argon- $\text{CH}_4$  mixture commonly used is  $5\text{ cm}/\mu\text{s}$ , a 1 ns measurement corresponds to  $50\mu\text{m}$  in y.

momentum. The average value is  $\langle P_T \rangle \approx 0.5$  GeV/c. Thus, most hadrons are emitted at small angles while the muons of interest will have  $20 \leq \theta_{\text{scatt}} \leq 70$  mrad. Except for the small fraction that are scattered horizontally, close to the median plane, most of the muons will leave tracks well above or below the median plane over a considerable fraction of their  $\geq 4$  meters of measurable length. With TPC measuring chambers spaced 0.8 meters apart, we anticipate no difficulty in identifying the muon track in all but the small fraction that will have tracks close to the median plane.

The typical charged hadron in the shower will be a pion moving forward thru the target until it interacts (absorption length in Be  $\approx 37$ cm) and produces its own secondary shower. As a general rule, the number of  $\pi^0$ 's produced is equal to the number of pions of either sign. Thus, as the cascade proceeds it becomes increasingly electromagnetic in character. Low energy pions and electrons will be bent by the magnetic field either to the right or left according to their sign. They will traverse the air gap and continue the cascade in the coil assembly and the iron yoke. A small fraction of the particles in the yoke may reenter the gap because the magnetic field in the yoke is of the opposite sign. Such hadronic showers have an absorption length which is <sup>(5)</sup>

$$L_{\text{abs}} = (203 \pm 21) + (91 \pm 8) \log_{10} (E/100 \text{ GeV}) \text{ gm.cm}^{-1} \text{ (in Fe)}.$$

Much of the energy of the shower will be dissipated in the target or converted to low energy particles in the cascade. What emerges from the target will be close to the median plane, and of energy low enough to be swept into the yoke within a few meters of the vertex. We expect

the TPC's will have sufficient spatial resolution to identify the muon from the remaining more energetic particles of the hadronic cascade. With good vertical focusing of the beam, we can expect that most of the hadronic shower will be contained within just a few cm of the median plane.

#### 11. Gated Time Projection Chamber

In our arrangement the muon beam passes through the time projection chambers. Moreover, we plan to use them to measure the incoming as well as the scattered muons. To avoid an excessive accumulation of positive ions we have developed a gated TPC. In our design, shown in Figure 9, we have introduced a gating grid in the drift region, 3mm above the cathode. This grid is normally biased somewhat positive with respect to the cathode. In this condition electrons drifting through the drift space toward the sense wires will be trapped between the gating grid and the cathode. They will be unable to reach the sense wires and hence positive ion formation will be suppressed.

When an acceptable trigger is received, the gating grid will be pulsed negatively with respect to the cathode so as to establish the normal drift field between them. In this condition the electrons from the particle tracks are brought to the sense wires in the normal way. With a 3mm space between the gating grid and the cathode a pulse of only slightly more than -45 volts (cathode at ground potential) is all that is required to establish a drift field of 150 volts/cm used with the standard Argon-CH<sub>4</sub> mixture. The wires of the gating grid are placed directly above the cathode wires to keep the capacitive coupling to the sense wires as small as possible.

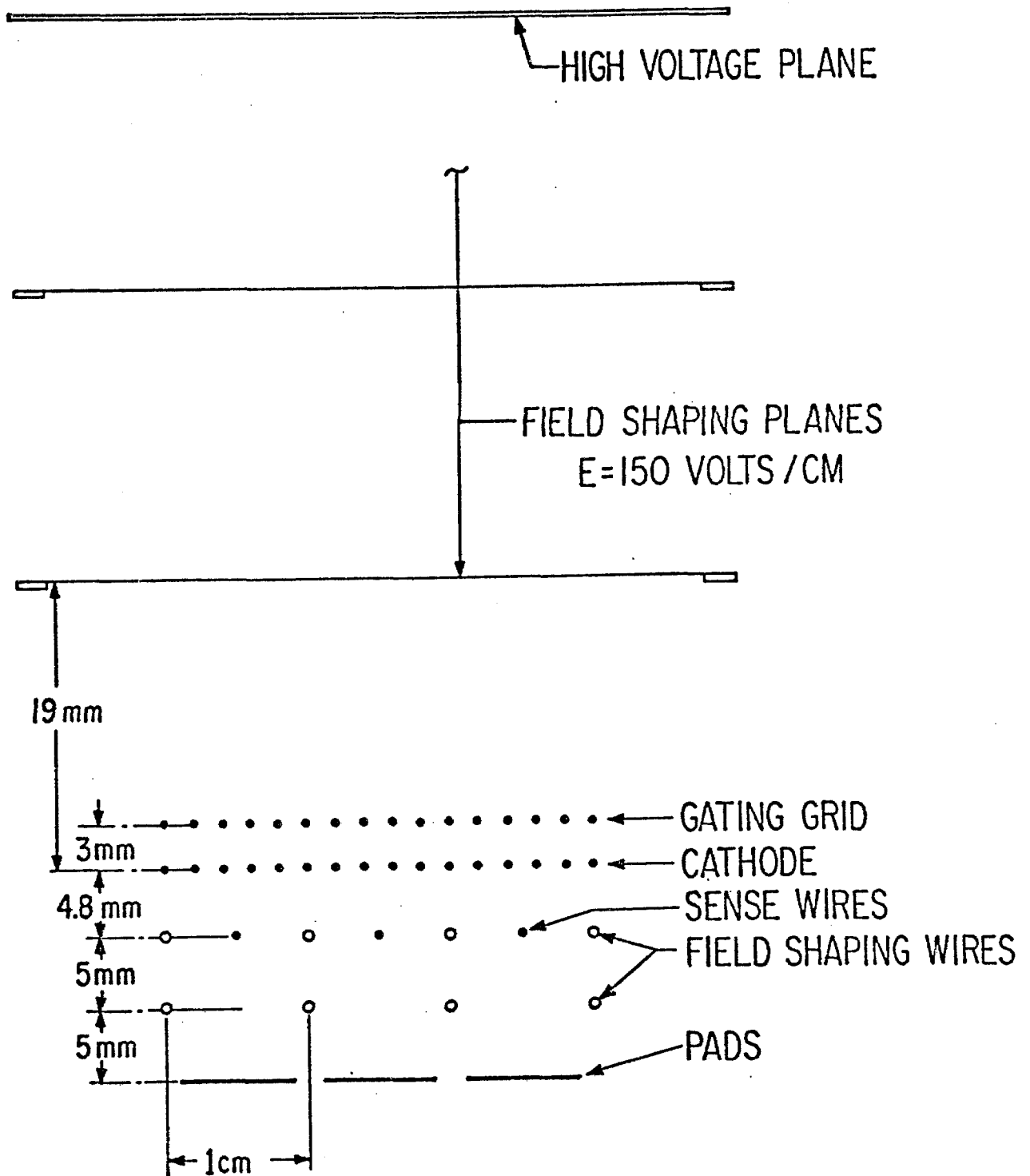


**Figure 10: Gated Time Projection Chamber:** The gating grid is normally biased slightly positive with respect to the grounded cathode. A negative 45 volt pulse on the gating grid establishes a uniform drift field up to the cathode and the TPC operates in the normal fashion. Delayed gates with small time windows based on trigger information limit the number of unwanted tracks read out.

The gate is operated in a different mode according to the type of trigger received. The objective is to minimize the accumulation of positive ions at the sense wires by limiting the number of drift electrons that can reach them. For the normal muon trigger in which the scattered muon is detected well above the median plane, the gating grid is turned on in the upward drifting chamber first and in the downward drifting chamber after a  $9\mu\text{s}$  delay. This allows the muon track which will be the first to be read out in the upper chamber to be recorded before beam track electrons appear. For the down drifting chamber we wait until the electrons from the beam region have been trapped by the gating grid and then proceed to read out the desired track information.

This type of gating is used for a group of chambers immediately upstream of the entry point to the muon trigger. It will give clean information on the scattered muon. To obtain clean data on the incoming muon we use a delayed gate turned on for about  $2\mu\text{s}$  on the chambers further upstream. This will record only the incoming beam particles. By limiting the gate opening to  $2\mu\text{s}$  the number of beam particles that would be read out would be of the order of 20 for  $10^7$  muons/sec in the beam. This is a manageable number in the TPC.

For triggers from muons near the median plane, we adjust the delays and narrow the width of the gate in the up and down drifting chambers to keep the read out time window as narrow as practical. We anticipate no difficulty in handling the 20 beam muons that would enter a  $2\mu\text{s}$  gate. In any case these load only the central pads. The scattered muons (and the accompanying shower particles) are read from the noncentral pads.

In the gated off position, the grid shields the anode from ionization electrons and prevents formation of positive ions. However, since the grid will be gated on only for the few microseconds necessary for the anode to collect the drifting charge from an event, it will be restored to the off position soon enough to trap the positive ions from that event and drive them to the cathode. Thus, the drift space is kept virtually free of positive ions which would otherwise distort the drift field and limit the precision of the readout.

## 12. Trigger Rates and Backgrounds

Our spectrometer is sensitive to a large fraction of the possible muon scatters. This causes a problem because of the large number of small angle scatters at low  $Q^2$ . These occur at the level of  $4 \times 10^{-3}$  of the photonucleon cross-section, or about  $0.5 \mu\text{b}$ . As a consequence, with a 50 meter Be target,  $3 \times 10^{-3}$  of the muons in the beam will scatter and become a potential trigger. In addition,  $\mu$ -e scatters contribute an additional  $1 \times 10^{-3}$  to the fraction of the beam that could produce a trigger in our geometry. For beams of  $10^7 \mu$ 's/sec, instantaneous rate, these scatters are capable of producing a trigger rate of  $4 \times 10^4$  per second, clearly excessive for any reasonable readout systems. A reduction by a factor of at least 100 is called for.

The distinguishing feature of these scatters is that they have rather flat trajectories which keep close to the median plane. The magnetic field in the gap bends them away from the beam, but after they enter the iron yoke they are bent back again. By the time they

reach the outer edge of the yoke they are moving in a direction almost parallel to the beam again. This is because  $(\oint B \cdot dl)_{\text{gap}} \approx (\oint B \cdot dl)_{\text{iron}}$ . Such muons can be identified by a multiple coincidence among rather small scintillators at the median plane near the outside of the yoke. Using this as a veto acceptable trigger rates should be obtained. The loss of good events by such a veto will be small but measurable. The method is to remove the veto during a 100 $\mu$ s gate. This will give a manageable number of events in which good events are represented with full acceptance. From such events the fraction lost will be determined.

The trigger is arranged to be insensitive to halo muons traversing the iron. The trigger counters are staggered and arranged to identify muons that move outward through the iron at angles considerably greater than the halo muons will have. Thus, accidental coincidence between halo muons and beam muons will not produce an appreciable trigger rate.

False events may be generated by muons from the decay of the pions (or kaons) of the hadron shower. Such pions are emitted with small transverse momentum  $\langle p_T \rangle \approx 0.5$  GeV/c. They will, therefore, stay close to the median plane. They behave like the low  $Q^2$  muons that produce them but add only fractionally to the number of low  $Q^2$  muons we have to deal with anyhow. However, since this mechanism produces opposite sign muons with equal frequency it will be necessary to install our veto scheme on both sides of the yoke. The analysis of the data with veto off will tell us how many wrong sign muons there are. We anticipate no difficulty in developing a detailed design of these trigger arrangements.

13. Cost Estimate

Cost per single 6m unit, in k\$.

1. Superconducting coils (from Appendix A)	300
2. TPC, 7 chamber pairs, 1120 pads @ \$50 ea.	56
3. Flash encoder readout, 1120 pads @ \$100 ea.	112
4. Data acquisition electronics	56
5. Trigger scintillators and PM tubes	
92 @ 500 ea.	46
6. Drift chambers, 450 wires @ 100 ea.	45
7. Beam hodoscopes	5
	<hr/>
	620

Total system, 10 6m units

1. Superconducting coils	3000
2. Refrigerators and power supplies	1000
3. Iron yoke (if Cosmotron steel is not available)	1250
4. TPC and Trigger Data Acquisition	3200
5. Installation Costs	500
6. Contingency	1000
	<hr/>
	9950

Total

9950

Estimated cost for an experiment with 12 meter target and 4 magnet modules with 1/2 the statistical accuracy

\$4,000,000

#### 14. Schedule

- |   |          |
|---|----------|
| 1. Complete detailed design of superconducting magnet                         | Oct 1981 |
| 2. Complete construction of prototype TPC chambers                            | Oct 1981 |
| 3. Complete construction of 1 6m unit: superconducting magnet and TPC readout | Jan 1983 |
| 4. Complete the full spectrometer ready to operate at Fermilab                | Jan 1985 |

#### 15. Beam Requirements

Our estimates are based on a total integrated luminosity of  $10^{40}$   $\mu$ 's  $\times$  nucleons/cm<sup>2</sup>. With the 50 meter Be target we plan to use, this translates to  $2 \times 10^{12}$  muons for each sign and each energy. Our design should operate comfortably with a muon beam of intensity  $\leq 10^7$   $\mu$ 's/sec. We anticipate  $\mu^+$  beams at 750 GeV of  $2 \times 10^6$ /sec in 20 second bursts every minute. This will require 833 hours of running time. For  $\mu^-$  the rates are down by a factor of 3, bringing the requirement to 2500 hours. Muon intensities are expected to be 3 times greater at 600 GeV. Thus the requirement is 278 hours for  $\mu^+$  and 833 hours for  $\mu^-$ . The complete experiment requires 4400 hours of good beam. Assuming a running efficiency of 50%, the experiment could be completed in 1 year's time, or 2 years if beam is available 1/2 the time.

## References

1. C.Y. Prescott, et al., Phys Lett. 77B, 347 (1978).  
C.Y. Prescott, et al., SLAC-PUB-2319, May (1979).
2. A.J. Buras and K.J.F. Gaemers, Nuc. Phy. B132, 249 (1978).
3. C.L. Wang, Phys. Rev. D10, 3876 (1974).
4. J. Ellis, "CHEEP, An e-p Facility in the SPS," CERN 78-02 (1978).
5. F. Siohan, et al., Nucl, Inst. and Meth. 167 371 (1979).

## MAGNET SYSTEM FOR 750 GeV MUON SPECTROMETER

### Introductory Remarks

The magnet field for the Time Projection Spectrometer should be 2 T in an unobstructed space of 0.8 x 0.8 m cross section and 60 m length. The field is vertical and transverse to the long direction. Outside the field is an iron shielding with a fourfold function: 1) selective shielding to identify and count muons, 2) containing the return magnetic flux, 3) improving field homogeneity, and 4) containing the magnetic forces. The field may be used in a dc mode, but from time to time the polarity will need to be changed from +2T to -2T in a time span not shorter than 40 s (being the interval between beam pulses); however, a slower ramp rate is acceptable. It is important that the overall cost of the magnets be as low as possible.

The present values of 2T in a 0.8 x 0.8 m space are largely determined by the availability of surplus iron, fitting this geometry. Other dimensions might be equally useful for high energy physics. Thus 0.5 T in a 3 x 3 m space has been suggested. An optimization study would be of interest, with the trade-off between field size and volume in mind. In an optimization the cost of the TPC counters will figure too.

For present day superconductor technology a field of 2 T is not particularly demanding, nor are the requirements for slowly ramping the field or for the field homogeneity (approximately 1% over the cross section of 0.8 x 0.8 m). Special design problems are posed by the saddle coil geometry and by the force containment. The challenge is to find a design combining economy with the necessary reliability. The choice of the cooling method and the conductor configuration also require optimal solutions.

The difference in electric power consumption favors superconducting over conventional magnet technology. A conventional copper magnet of 60 m length would consume between 10 and 30 MW, the superconducting version needs only about 60 kW refrigerator power. At 5¢/kWh the difference in the power bill for one run of approximately  $3 \times 10^6$ s operation time would amount to between 0.4 and 1.2 M\$. The power cost in one year would be more than the difference in capital cost between the conventional and the superconductive magnet version.

### General Description of Magnet Design

A conceptual design for a superconductive 2 T magnet has been made. The magnet is composed of units of 6 m length. Each unit, being self-contained and encased in a single vacuum shell, has two halves, top and bottom, with saddle crossings at both ends. Each unit has 796 turns of a conductor consisting of a multifilamentary NbTi-Cu composite, combined with enough copper to give a Cu:SC ratio of 16. The conductor cross section is square, 5.7 x 5.7 mm. The coil current is 2 kA for a 2 T field.

The coil windings are composed of 44 largely identical subunits, stacked on top of each other. Each subunit is wound flat as a 22 turn pancake on a window frame of 1.7 x 6 m and afterwards bent into the required saddle shape. The window frame coil-form is of copper. Cooling is by circulating two-phase

helium through copper pipes attached to the coil forms. If all the magnetic energy of  $\sim 9$  MJ per 6 m unit were dissipated in the cold mass of winding and structure of approximately 6 tons, the temperature would increase from 4 K to about 40 K. The windings are not potted; thus they can adjust to the elastic deformation of the load bearing structure while the coil is energized. Potting would be complicated and expensive, and it would entail a great risk of cracking under the strain caused by the increasing field.

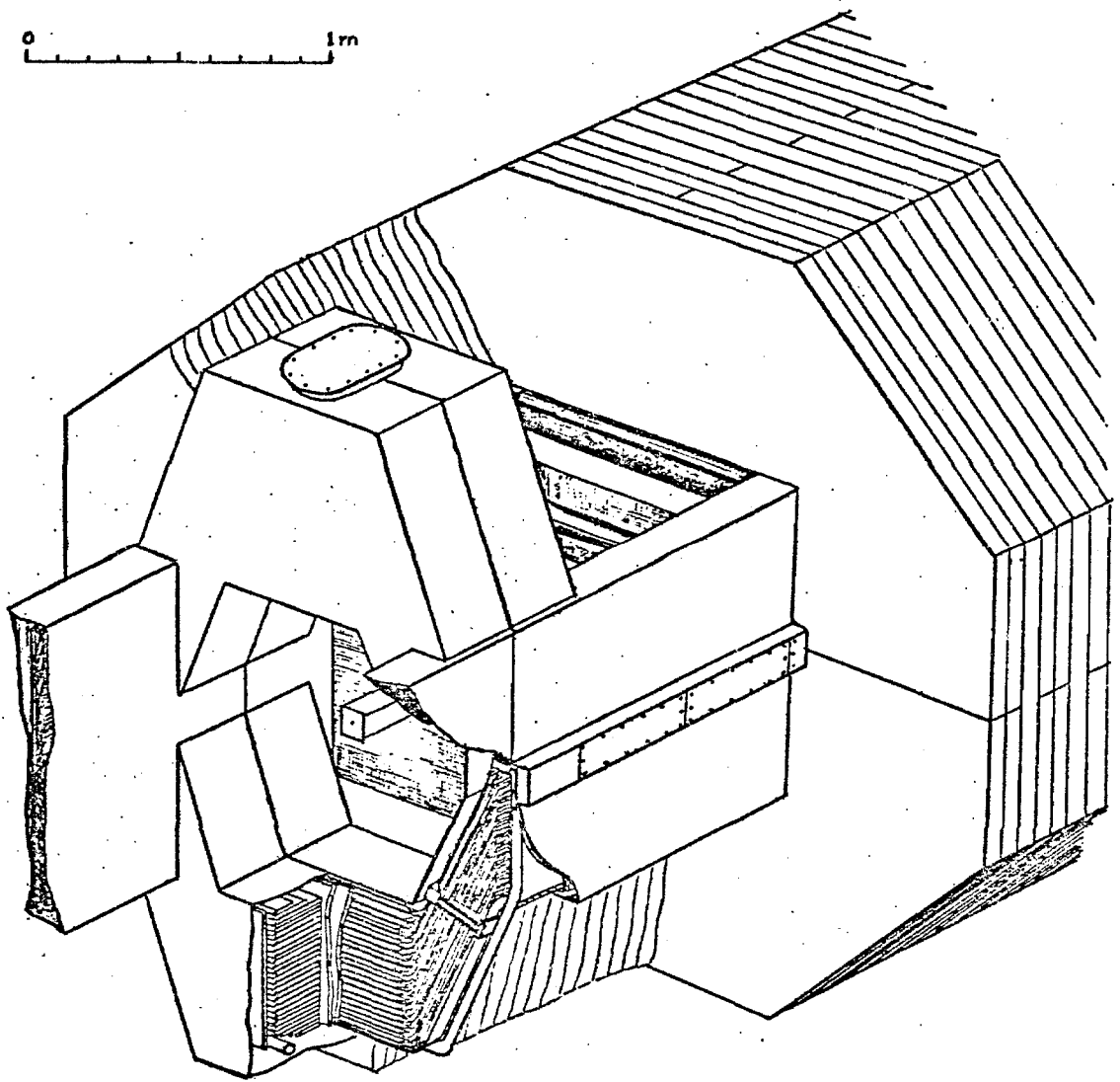
The forces are contained by tension members at 4 K which connect the two sides of the coil at top and bottom and carry about half the force. The other half of the force, about  $8 \times 10^5$  N per m length at 2 T, is taken from the middle of the windings through special supports from 4 K to room temperature to the iron shield serving as a C-clamp. The weight of the cold parts of the coil, are suspended by stainless steel wires. St. steel wires also center the coils relative to the iron shielding. Warm pressure supports are also necessary for the saddle crossings, especially at the two end units, but also for the other crossings, in case one of the units is switched off. The structure is allowed to deform elastically by about 3 mm before touching these warm supports. Thus there is only a heat leak through these supports when they also transmit force.

The superconducting operating mode at 4 K is fully stable up to approximately 2200 A current; this means that the minimum propagating zone is infinitely large up to this current. The quench current is estimated to be above 2500 A.

The total refrigeration load is approximately 120 W at 4 K, if central warm supports are used, and about half that much if all forces are handled by cold tension members. The heat leaks at 4 K are 7 W per 6 m unit through the cryostat walls, which have superinsulation of 2.5 cm thickness including a 70 K shield; another 5 W are through the central warm supports when the coil is energized. Two refrigerators of 100 W capacity at 4 K can handle the total refrigeration load at 4 K (e.g. CTI 1400). The room temperature power required is about 35 kW for each. The total heat load at 70 K is 1100 W requiring another similar refrigerator.

In summary: the design principles are based on economy and reliability. The modular design has each of ten 6 m units composed of stacked, largely identical subunits, easy to wind. The cooling is indirect; heat from the superconductors is removed by conduction to circulating two-phase helium. A very conservative stability criterion is used to give a comfortable safety factor for the superconducting operation. The design includes many original features.

In an appendix are discussions of design details, covering: a) conductor, b) assembly of coils, c) superconductor stability, d) eddy current losses, e) protection, f) cooling, g) refrigeration, h) vacuum shells, i) forces, and k) cost estimate; and some tables of data.



GENERAL VIEW OF MAGNET , junction of two 6m units

Design details of magnet system for 750 GeV muon spectrometer.

## a. CONDUCTOR

To get a field of 2T a current of 1.6 MA turns/m is necessary. The choice of operating current is guided by ramp rate voltage limitations, by the requirements of current leads between room temperature and 4 K, and by ease of handling the conductor for winding, current connections, manufacture. A current of 2 kA seems most suitable. With a stored energy of 8.64 MJ per 6m unit the inductance for a 2 kA conductor with 796 turns is 4.32 h. The coil voltage becomes 125 V for a charging time of  $\Delta t = 80$  s ; with all 10 6m units in series the voltage of 1250 V is quite manageable. A charging time of 80 s allows the reversal of the field in 160 s; in this interval two accelerator beam pulses, lasting 20 s every minute, will be missed. Shorter charging times of  $\Delta t = 50$  s , missing one beam pulse during reversal, or  $\Delta t = 20$  s for reversal between beam pulses might be desirable but are not recommended for the present magnet design. The series voltage of 2 kV for  $\Delta t = 50$  s or 5 kV for  $\Delta t = 20$  s can be contemplated. More serious problems would be the eddy current losses in the cold structure surpassing the refrigerator capacity, and the considerable power consumption for frequent reversals if the magnetic energy has to be dumped.

The proposed conductor is composed of 16 wires of 0.635 mm diameter each having 360 superconducting filaments of 20  $\mu$ m diam NbTi in a copper matrix ( Cu:SC = 1.8 ) the filaments being twisted with a twist pitch of approx. 2 cm. . The 16 wires

are stranded around a pure copper core of square cross section, 2 x 2 mm, with a pitch of approx. 5 cm. The conductor is completed by two layers of copper wire of 0.7 mm diameter, the first layer of 24 wires having the pitch parallel to the superconducting wires, the final layer of 32 wires having an opposite pitch. The core and all wires are solder coated ('Staybrite' or indium) before stranding. The solder is melted and the excess removed while the conductor is compacted and sized to be exactly 5.7 x 5.7 mm. The overall Cu:SC ratio is 16:1; with a critical current density of the superconducting filaments of  $j_{sc_0} = 3.3 \times 10^5$  A/cm<sup>2</sup> at 2 T, the conductor short sample critical current becomes 6000 A. The conductor is insulated by a single wrap of 1 mil Kapton. See Fig. 1 .

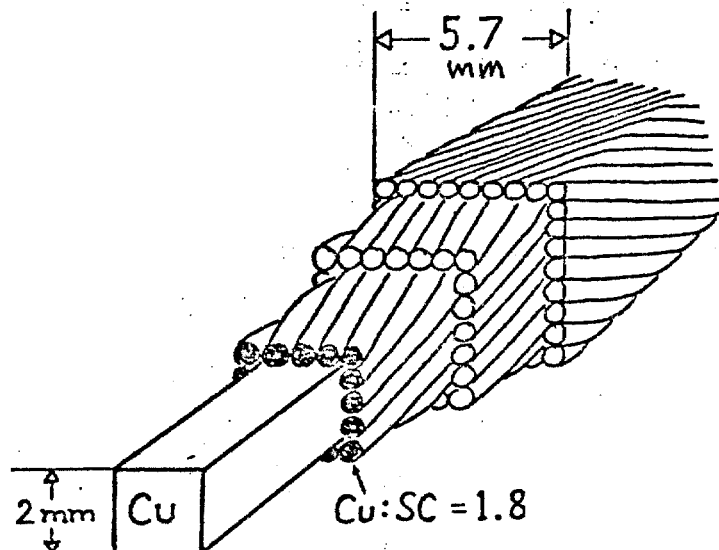


FIG. 1  
The conductor

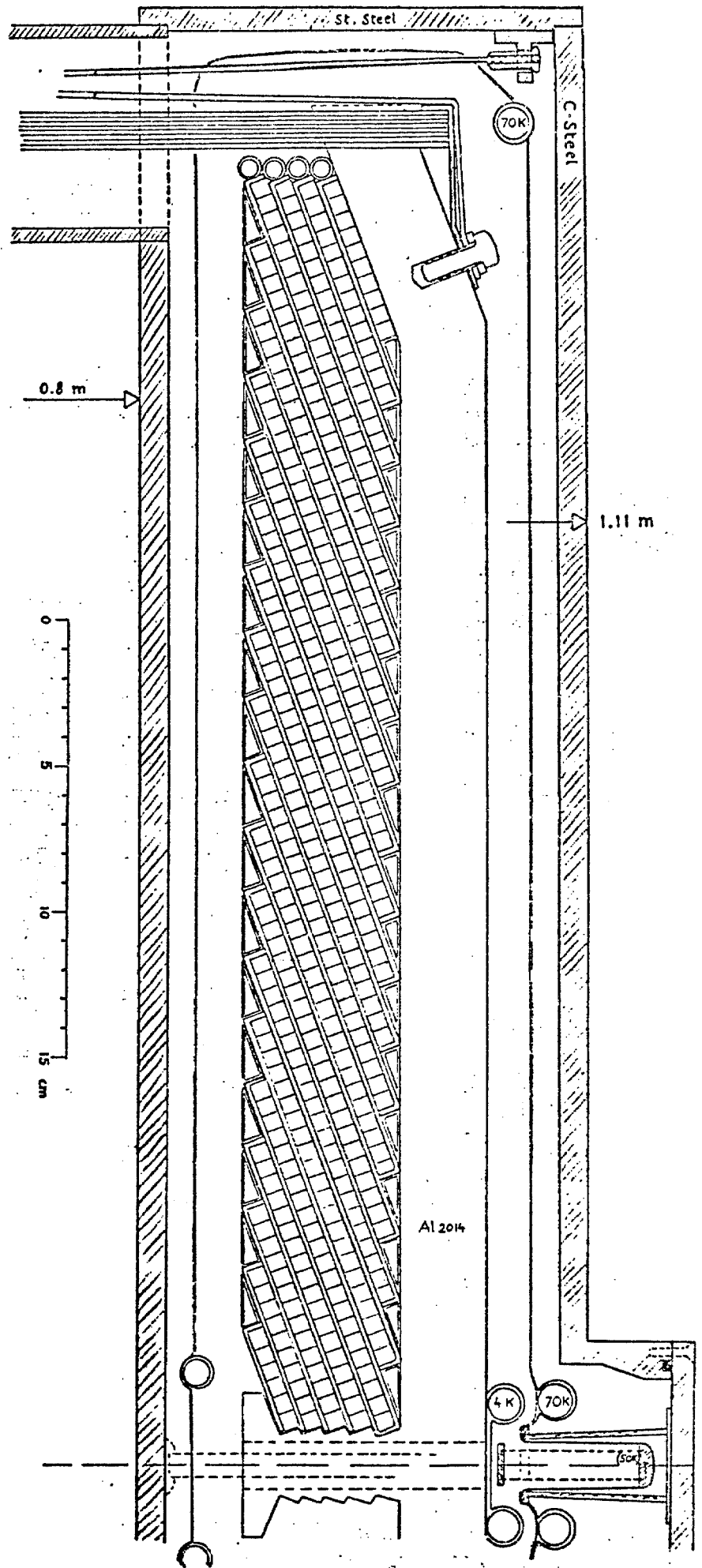


FIG. 2  
Cross section of  
winding quadrant

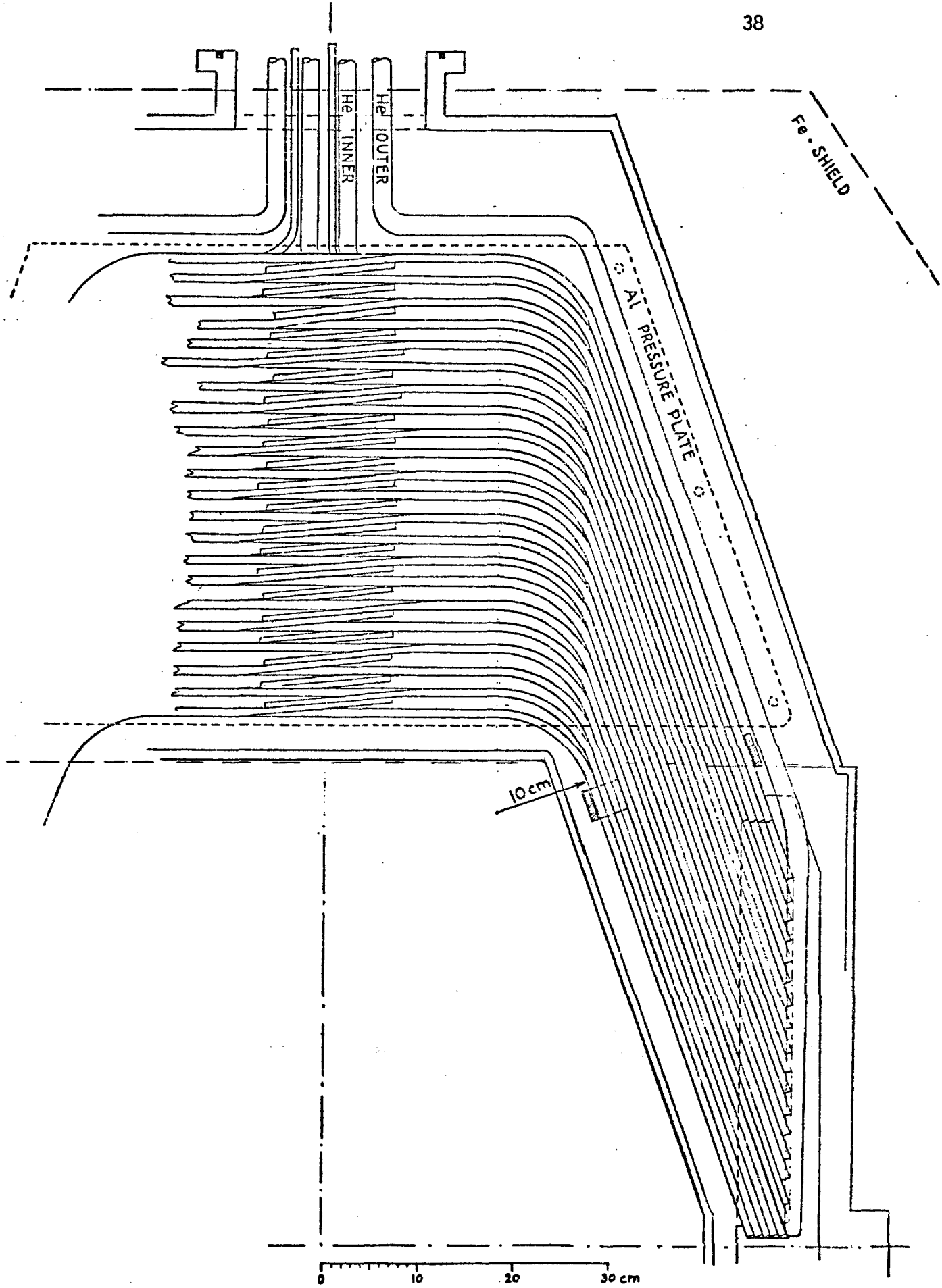


FIG. 3 View of crossing

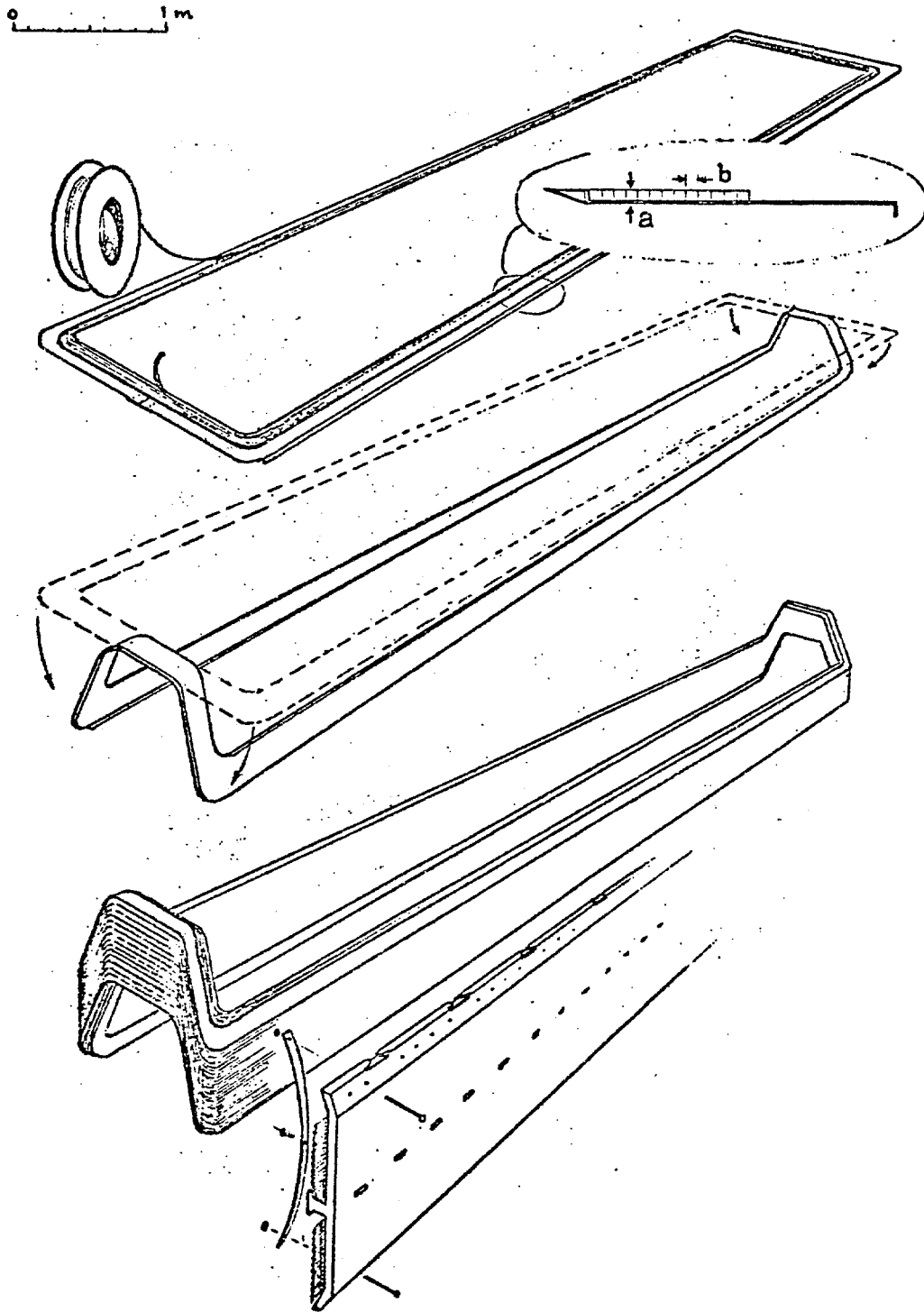


FIG. 4 Assembly of coils

## b. ASSEMBLY OF COILS

Each half of a 6 m unit consists of 22 single layer coils stacked on top of each other. Of these individual subunits 13 are identical and the remaining 9 deviate in minor details and have fewer turns. A cross section of the coil and a view of the crossing are illustrated in figures 2 and 3. The assembly procedure is illustrated in fig. 4 .

1. The individual coils are wound as flat window frame pancakes; half of them are wound clockwise, half of them counter clock-wise. The standard coil has 22 turns. The smaller coils have 18, 14, 10 and 6 turns and the same inside dimensions; these fill the inside corners of the stack. The coils for the outside corners have 18, 14 and 10 turns and the same outside dimensions as the standard coil; these also have round cooling tubes, while all others have cooling tubes with triangular cross section.

2. The coils are bent around a 10 cm radius to an angle of 70°. The angle is given by the exact dimensions of wire, insulation and coil form:

$$\cos \chi = d/(4b) , \text{ where } d^2 = 4[2b^2 + b(4b^2 - a^2)^{\frac{1}{2}}]$$

d is the vertical translation from one coil to the next, and a and b are dimensions indicated in Fig. 4 .

3. The coils are stacked, using 1 mil Kapton sheet for insulation between coils (in addition to the insulation provided by the Kapton wrapped on the conductor).

4. The stacks are combined with the Al-pressure plates. The pressure plates also form part of the inner vacuum shell, which is completed by 1 mm Al-sheet. After completion of this part

of the inner vacuum shell, clamps in the form of  $\frac{1}{4}$ " thick G-10 strips are applied every 20 cm of the length of the pressure plates. The original curvature of the G-10 strips provides a slight pressure on the assembled coil, important to heat transfer by contact. The G-10 strips also give sufficient strength to the inner vacuum shell. Clamping around the inclined legs of the crossings is illustrated in fig. 5.

6. Before finishing the inner vacuum shell the end connections to inner and outer cooling tubes and the current connections between the stacked coils are made.

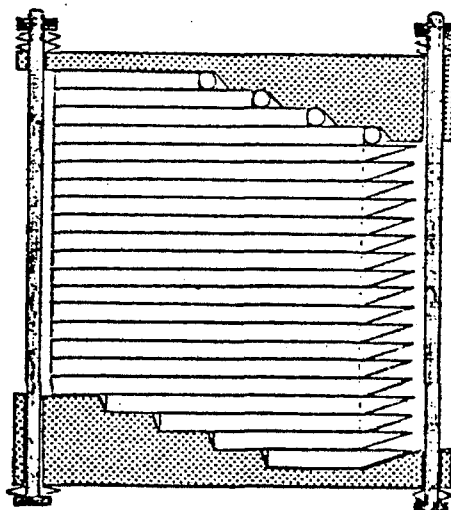
7. Throughout the assembly it must be kept in mind that all current conductors are to be in physical touch with cooled elements. This is especially important in the area of the crossings with all the current connections and current leads.

Two assembly principles will help to insure success:

i. all clamping should be elastic to insure contact when the coil is not energized; ii. when the coil is energized all Lorentz forces should be directed to and counteracted by actively cooled elements of the structure.

FIG. 5

Clamping of inclined legs of crossings using G-10 brackets and spring washers



### c. SUPERCONDUCTOR STABILITY

The stability of operation in the superconducting state is of some importance. A reliable indication of stability is the size of the minimum propagating zone (MPZ). For full stability the MPZ must be infinite. If the MPZ is finite superconducting operation is maintained as long as the energy needed to create the MPZ is larger than the energy available from energy releasing disturbances occurring within the windings.

Three types of MPZ may be considered (see fig.6).

- i. Single conductor: the length of a normal zone that is just large enough to propagate (analysis: transmission line case, ref.1)
- ii. Single layer: the number of turns to be normal before propagation to neighboring turns occurs. (transm. line case, ref.1)
- iii. Whole winding: the volume of winding to be normal before propagation occurs (analysis: spherical case, ref.1).

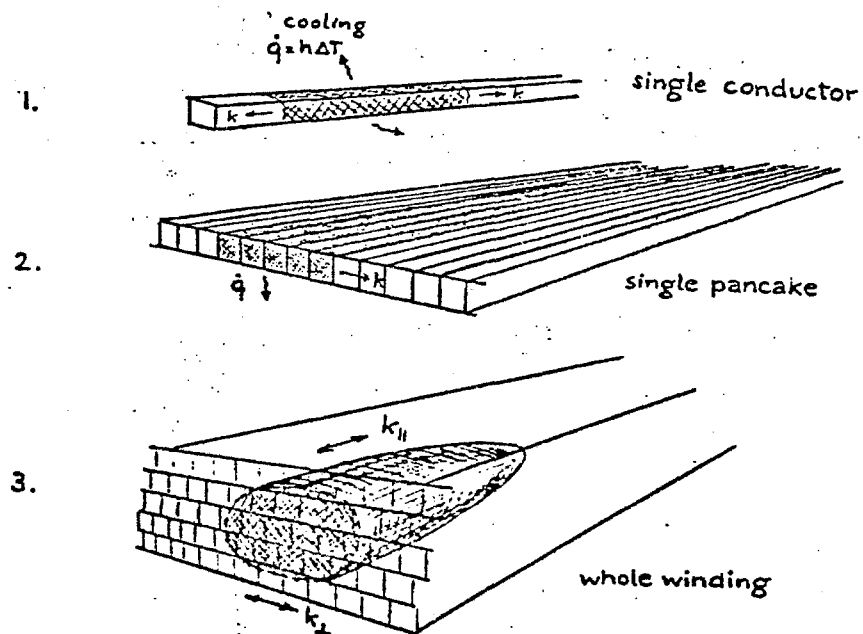


FIG. 6 Different cases of Minimum Propagating Zones

The thermal conductivity of the conductor will be  $k_u = k_{Cu} = 10 \text{ W/cm K}$ . The insulation has  $k_{ins} = 10^{-3} \text{ W/cm K}$  and thickness  $d_{ins} = 0.1 \text{ mm}$ . The heat transport through the insulation into the copper coil form is represented by a heat transfer coefficient:  $h_{ins} = k/d = 0.1 \text{ W/cm}^2\text{K}$ . If heat transport from turn to turn is considered an effective thermal conductivity  $k_1 = k_{ins}(d_{cond} + d_{ins})/d_{ins} = 5 \times 10^{-2} \text{ W/cm K}$  is active.

One can never assume that 100% of the surface is in ideal contact for heat conduction. We assume 20% and use as effective values:

$$h_{ins} = 0.02 \text{ W/cm}^2\text{K} \quad \text{and} \quad k_1 = 10^{-2} \text{ W/cm K}.$$

For cases i. and ii. the formulae of the so called transmission line geometry (see ref.1) are used. Stability is characterized by two parameters:

$$\xi_j = \frac{h}{R_s} \frac{T_j - T_o}{\rho j^2} \quad \text{and} \quad \xi_o = \frac{h}{R_s} \frac{T_c - T_o}{\rho j_o^2}$$

with  $R_s$  being cross section / cooled perimeter.

The following values are used:  $T_c = 9.5 \text{ K}$ ;  $T_j = 7.7 \text{ K}$ ;  $j = 6.2 \text{ kA/cm}^2$ ;  $j_o = 1.85 \times 10^4 \text{ A/cm}^2$  (at 2T);  $\rho = 10^{-8} \Omega\text{cm}$ ; in case i.:  $R_s = b/4 = 1.45 \text{ mm}$ ;  $h = 0.02 \text{ W/cm}^2\text{K}$ ;  $k = 10 \text{ W/cm K}$ ; in case ii.:  $R_s = b/2 = 2.9 \text{ mm}$ ;  $h = 0.02 \text{ W/cm}^2\text{K}$ ;  $k_1 = 0.01 \text{ W/cm K}$ . We obtain in case i:

$$\xi_{j0} = 1.3 ; \quad \xi_{o0} = 0.22$$

in case ii.:

$$\xi_{j0} = 0.68 ; \quad \xi_{o0} = 0.11$$

A stability parameter of  $\xi_j \geq 0.5$  means that the MPZ =  $\infty$  and stability is fully stable. The indication therefore is, that the coil winding is fully stable at the operating current.

The stability for a single wire seems to be much higher. However, if a single wire is only cooled by contact along one of its surfaces (instead of all four as assumed above), the stability parameter drops to  $\frac{1}{4}$  and becomes  $\xi_j = 0.325$ . This means it is MPZ-stable, i.e. it can recover provided a normal zone does not exceed the length of an MPZ. At  $\xi_j = 0.325$  the MPZ for our conductor is 17 cm long. If the single wire (i.e. the section cooled on one side only) is shorter than that it is perfectly stable.

The stabilization parameter  $\xi_0 = 0.12$  means that full stability reaches to  $j/j_0 = 0.36$  (global stability to  $j/j_0 = 0.28$ ).  $j/j_0 = 0.36$  corresponds to  $I = 2.16$  kA.  $\xi_0 = 0.22$  indicates full stability to  $j/j_0 = 0.48$  (global to  $j/j_0 = 0.37$ ); but if only one face is cooled  $\xi_0 = 0.055$ , then full stability is up to  $j/j_0 = 0.28$  (global to 0.21). Full stability more detailed:  $0.5 \leq \xi_j < 1$  is MRZ stability;  $\xi_j \geq 1$  is global stability (see ref.2). MRZ-stable means that a device can recover from being fully normal except for a small superconducting portion called a minimum recovery zone (MRZ); at  $\xi_j = 1$ , MRZ = 0 and at  $\xi_j = 0.5$ , MRZ is nominally half the device.

The third case (spherical geometry) is approximated when the coolant is not active, that is for instance after all the helium is vaporized. In that case the MPZ is always finite. The MPZ becomes ellipsoidal, with  $R_{crit} = [3k(T_j - T_0) / \rho j^2]^{\frac{1}{2}}$ .

In the direction parallel to the conductor one gets  $R_{crit} = 17$  cm, across the conductor  $R_{crit} = 0.44$  cm, with a volume of  $13.8$  cm<sup>3</sup>. The MPZ, then, is roughly equivalent to two neighboring conductors being normal for a length of 21 cm. The energy required to produce such a normal zone is approx. 0.15 J.

A word about disturbances. The coil is assembled dry, and the windings are therefore free to move under the influence of magnetic forces, provided such motion is allowed by the structure or is necessary to even out the structural reaction. Thus, big motions at highest currents due to breaking of rigid bonds - a cause for training in many coils - are avoided. Any stick-slip motions ought to be very small. Furthermore, in the present design the highest pressure is near the pressure plate where the field is lowest and vice versa the windings in a high field are under lower pressure.

Nevertheless, we should consider orders of magnitude for the disturbances. At 2T the highest pressure is 1.6 MPa. For a motion of 0.1 mm this corresponds to an energy of  $16$  mJ/cm<sup>3</sup> equivalent to the enthalpy difference of copper between 4 and 9 K. The highest Lorentz force is at 2 T and amounts to 40 N per cm of conductor. A motion of 0.1 mm of one conductor relative to its surroundings can release a maximum of  $12.3$  mJ/cm<sup>3</sup> or the enthalpy difference from 4 to 8.5 K if all the energy is dissipated in the conductor.

The stability appears to be very high. It depends, however, very strongly on the actual heat conduction. Since stability is only needed when all magnetic forces are highest, it is possible that the initial assumption of only 20% contact may

be too pessimistic, and stability is even higher than calculated. Only some separate experiments prior to the final designing of the coil can give the necessary data.

The stability as calculated above assumed heat transport by direct contact only. Under this assumption the inner vacuum shell would not be necessary. The only purpose of the inner vacuum shell, if it should indeed prove necessary, is to allow the presence of helium gas at low pressure as a heat exchange medium to improve the heat transport within the windings.

#### d. EDDY CURRENT LOSSES

A changing field would induce large currents flowing in the coil forms if they were allowed to form a single electrically shorted turn. The single turn resistance of all the copper including cooling pipes would be only  $1.6 \times 10^{-7} \Omega$  and the energy loss during ramping  $\Delta\Phi^2/(R \Delta t)$ . With  $\Delta\Phi = 10.6$  Vs for 0 - 2 T the losses would be prohibitive. The coil forms are therefore made in two electrically separated halves connected by means of G-10 plates at the middle of the crossings.

The inner vacuum shell too should be interrupted by an insulating section at the crossings.

At the fastest ramp rate of  $\Delta t = 80$  s, the loss in the copper coil forms due to the magnetic field penetrating the windings is estimated to be about 60 W for a total of 5 kJ per 6 m unit. With the planned refrigerator capacity such losses can easily be absorbed provided the field reversals are not more

frequent than once every 15 minutes.

e. PROTECTION

In case of a quench the high thermal conduction throughout the winding will prevent the formation of hot spots. If necessary the cold mass can absorb the total magnetic energy resulting in a final temperature of around 50 K, that is assuming all the helium has boiled dry before the quench. However, the usual protection scheme of shorting the coil through an external resistance upon detection of excessive resistive voltage at the terminals recommends itself. The voltage level before triggering the protective switch can be as high as 10 or 20 V; this makes distinction between inductive and resistive voltage simple.

f. COOLING

Indirect cooling of the windings has been used very successfully in other large superconducting magnets (ref.3, 4). Cooling is needed for cooldown and for maintaining superconducting operating temperature. At operating temperature, chosen as 4 K, heat from the following sources has to be removed;

- steady heat leak through cryostat walls
- heat leak through force supports, depending on magnet being energized.
- eddy current losses during ramping of the field
- resistive heating at conductor joints and from temporary resistive zones in the wake of disturbances

- heat leaks through current leads.

Most of the cooling is done by the inner and outer set of cooling tubes associated with the windings. The inner set consists of the copper tubes connected to the coil-form copper sheets, the outer set are the aluminum tubes attached to the pressure plate. With few exceptions these tubes have a triangular cross section. Each set of tubes in the top and bottom half and on each side is connected in parallel forming together 8 separate circuits in each 6 m unit. Inner and outer sets are thermally well connected through the winding structure and top and bottom sets are connected by the pressure plates. For superconducting operation inner and outer sets will be used in counterflow; for cool-down the coolant flow in all 8 sets will have the same direction. The coolant flow will be adjusted to the load. The coolant is two phase helium at 4 K (slightly below atmospheric pressure). The helium inventory is 23 l per 6 m unit.

#### g. REFRIGERATORS

Refrigeration is provided by two refrigerators each of 100 W capacity at 4 K and by one refrigerator of 1.8 kW capacity at 70 K. The 4 K heat load for steady operation will be around 12 W per 6 m unit with 6 W through cryostat walls, 5 W through force supports and 1 W from the conductor joints and leads. For ten units this amounts to 120 W, needing the evaporation of 6 g/s of liquid helium, or 170 l/h with the vapor returning at close to 4 K to the refrigerator.

The total length of the cooling circuits is 66 m per 6 m unit,

consisting of 4 inner and 4 outer parallel tube sets of 7.6 m each and 6 m of connections ( $\sim 3$  cm ID). Each of the 8 circuits per 6 m unit will be series connected to the same circuit in the neighboring units. Thus 8 main circuits run the length of all ten units. Each of the refrigerators is connected to half of these; the four are in parallel for cooldown or in series for superconducting operation, as indicated in fig.7., with the following advantages:

- cool-down if necessary with one refrigerator only
- maintaining low temperature is also possible with one refrigerator only
- inside has better cooling than outside (inside has 2 T, outside 0 T)
- superconducting operation with one refrigerator if necessary (possibly at somewhat reduced but still sufficient stability)

The pressure drop at flow of 6 g/s, (3 g/s from each refrigerator,) is estimated to be less than 300 Pa .

The heat leak into 70 K is approx. 110 W per 6 m unit. Approximately 80 W are through the warm supports and 30 W through the super insulation and leads.

Estimated cool-down time is 7 days (using no additional refrigerator).

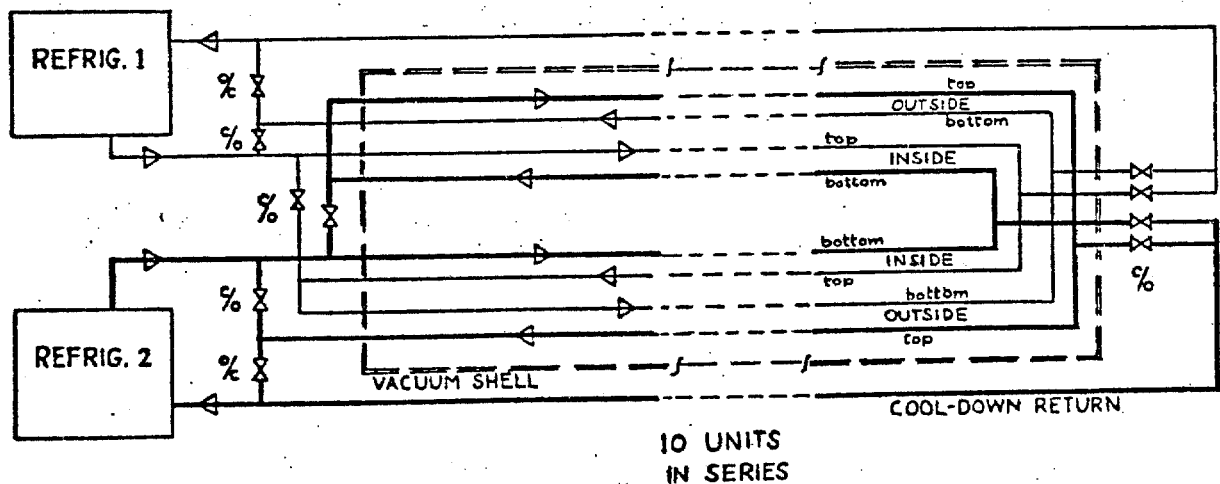


FIG. 7 Cooling circuits. Flow for maintaining low temperature is indicated. For cool-down all 10 valves are operated. (valve positions indicated; for cool-down the 4 valves on the right are open)

## h. VACUUM SHELLS

The outer vacuum shell is of stainless steel plates, welded together. The inner and outer plates are kept apart by central posts in order to support the atmospheric pressure without too much deformation. Plates of 1 cm thickness will bend inwards by less than 3 mm, whereas without central support plates of 1" thickness would bend through by as much as 6 mm at the center. The central supports have to carry  $10^5$  N/m or a total of  $6 \times 10^5$  N on each side; if posts are set every 40 cm their load will be 40 kN. The posts are made of G-10, cross section  $1.14 \text{ cm}^2$ , loaded to 0.35 GPa. In order to avoid buckling they have an H-profile. Suitable holes are in the central rib of the pressure plates to allow the central posts to be located without touching any 4 K structures. See Fig. 8.

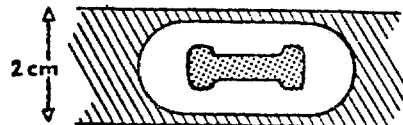


FIG. 8 Cross section of G-10 posts

It may be expedient to have bolted, O-ring sealed cover plates for each 36 cm force support unit, mainly for ease of assembly.

The inner vacuum shell is made of 1 mm thick aluminum sheet and soldered to the pressure plate and the central rib. The gas pressure inside the inner vacuum shell is only about 10 kPa. The main purpose of the inner vacuum shell is to allow the presence

of helium gas for improving the heat transport within the windings. If tests should prove that heat transport by contact is satisfactory, as it is expected to be, no inner shell will be necessary, or at least it need not hold a vacuum.

Superinsulation fills the space between inner and outer shell. On the average 50 layers of superinsulation are applied at 20 layers/cm. There is an intermediate temperature shield of 1 mm thick copper, cooled to a temperature of 70 - 100 K. The shield is located at approx 1 cm from the outer wall. At an average thermal conductivity through the superinsulation of  $\bar{k} = 0.3 \mu\text{W/cm K}$  the heat leak into 4 K becomes 6 W and into the intermediate shield 20 W .

## 1. FORCES

### 1. Magnetic forces

The magnetic pressure of 1.6 MPa is supported on each side by the pressure plate of 3 cm thick aluminum (2014 or 2024) weighing 480 kg. The left and right pressure plates are connected by cold tension struts at top and bottom, every 40 cm. In addition there are the warm supports at the center which transmit half the force to the wall of the outer vacuum shell at room temperature and hence through the iron shield acting as C-clamp to the opposite side. The total force on each side's pressure plate is 9.6 MN, 4.8 MN each on the top half and bottom half; half of this force, i.e. 2.4 MN is carried in the cold struts, the other half in the warm supports.

The cold tension struts carry 0.16 MN each and are of stainless steel stressed to 0.5 GPa. They are formed of 8 stacked st.st. sheets each 1.6 mm thick and 2.5 cm wide with T-shaped ends fitting into machined slots on the pressure plates. See Fig.9. They are located in 6.5 cm I.D. stainless tubes that connect the inside st. st. plates of the outer vacuum shell at top and bottom.

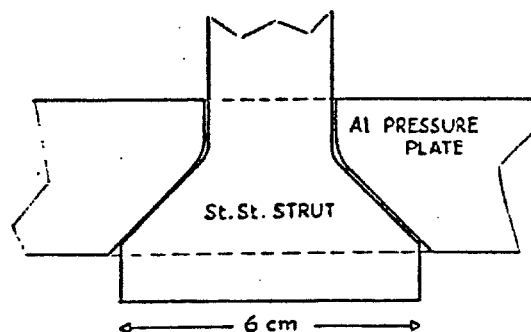


FIG. 9 Connection between tension strut and pressure plate

The warm supports are subdivided into sections of 36 cm fitting between the center posts that hold the outer vacuum shell's walls apart. Each of the 15 sections has to carry a maximum of 0.33 MN. The supports are composed of two pressure members connected by a tension member. The inner pressure member is cold, 4 - 50 K, consisting of a row of 8 polyester/glass-fibre pylons each of 1.1 cm diameter, 5cm long, carrying 40 kN at 0.42 GPa. The heat leak, with  $\int_4^{50K} k dT = 10 \text{ W/m}$ , is 19 mW. For the whole side with 120 pylons the leak becomes 2.3 W, or 4.6 W per 6 m unit. The outer pressure member is warm, 70 - 300 K, consisting of two G-10 plates, 1.5 mm thick and 5 cm x 36 cm, stressed to 0.3 GPa. The heat leak into 70 K will be 2.6 W for a total of 78 W per 6 m unit.

The inner and outer pressure members are connected by two stainless sheets, 0.8 mm thick, 4.5 cm x 36 cm, stressed to 0.58 GPa. The temperature drop across the steel sheets

( $k_{77} = 80 \text{ mW/cm K}$ ) carrying the 2.3 W flowing through the inner pylons becomes 21 K.

It must be mentioned that the pressure plates touch the warm supports only at currents above 280 A, when the pressure plate deformation reaches 2 mm at the center.

The possibility of carrying all the forces in cold tension, and without warm supports, would need a pressure plate of at least 7.6 cm thickness in order to keep the central elastic deformation below 5 mm. Such a solution is not considered viable because the extra space would go at the expense of the needed iron shield.

#### ii. Weights

The weight of the cold mass of 6 tons is carried by stainless steel bands, approx. 90 cm long, running from the bottom of the pressure plates to the top plates of the outer vacuum shell. The length between 4 and 70 K is at least 60 cm. Seven bands on each side, spaced 80 cm suffice. Each is 13 mm wide and 1.6 mm thick and carries 4.3 kN at a stress of 0.2 GPa. The heat leak, with  $\int_4^{70\text{K}} k \, dT = 2.6 \text{ W/cm}$ , is 9 mW per band and 0.13 W per 6 m unit.

#### iii. Centering

There are supports needed to prevent the coil from becoming unbalanced relative to the iron shield and therefore experiencing strong attractive iron forces. Horizontal st. steel wires go from the pressure plates to the top or bottom plates of the outer vacuum shell on the other side, at each location of a tension strut. Their length is 1 m, diameter 1.6 mm, they are prestressed

to about 200 N and have a yield strength of approx 1.7 kN each. They each have a spring constant of 2.7  $\mu\text{m}/\text{N}$ ; for the 60 wires this gives a total spring constant of 44  $\text{nm}/\text{N}$ , which is considered sufficiently stiff. The heat leak of all 60 wires, at  $\int_4^{300\text{K}} k \, dT = 35 \text{ W/cm}$  is 0.4 W.

On each side 7 wires from the top of the pressure plates to the bottom outer vacuum shell plate will restrain possible upward movement.

Centering in the long direction is done by similar wires attached to the middle of the 6 m unit. They are to insure that the thermal contraction of a total 2 cm length change between RT and 4 K is distributed evenly to give a movement of 1 cm at each end.

#### iv. Forces at crossings

The crossings are sandwiched between Al pressure plates 2 cm thick. The two end units need warm supports for the outward forces. These warm supports are similar to the central warm support described above.

The inner units are connected, their outer vacuum shells being joined. The neighboring crossings are connected by cold stainless steel members capable of acting in compression or tension, as needed if single units should be de-energized in emergency. These connections must have provisions to be lengthened by 2 cm after cooling, in order to compensate for the thermal contraction of each 6 m unit.

## k. COST ESTIMATE

(data for material and labor are given per 6 m unit; prices in k\$ )

Material

Conductor:	length (796 turns @ 15.4 m)	$1.23 \times 10^4 \text{ m}$	
	volume (NbTi: 0.0234; Cu: 0.375)	$0.4 \text{ m}^3$	
	mass (NbTi: 150; Cu: 3350)	3350 kg	
price of material:	NbTi (\$200/kg)		30
	Cu (\$ 5/kg)		17
			<hr/> 47
price of finished conductor	3 x material, or		
	\$12/m, or		
	\$ 4/kAm (at 5T)		150
			<hr/> ===
copper:	coil forms and cooling tubes,	1320 kg	6.5
aluminum 2014:	pressure plates, cooling tubes		
	1120 kg (\$ .2.2/kg)		2.5
stainless steel 304:	for tension struts	34 kg	
	for vacuum shell	1700 kg (\$ 2.5/kg)	4.4
C-steel:	for outer plates of vacuum shell	950 kg (\$0.7/kg)	0.7
G-10 (incl. polyester/glass-fibre):			
	for central posts, clamps, warm supports,	55 kg	0.25
			<hr/>
	total		164.35

Labor

winding	30
vacuum shell	20
superinsulation	10
helium ducts	10
current leads	10
supports, (assembly and test)	15
	<hr/>
total	85
Total of material and labor, + 20%	<u><u>300</u></u>

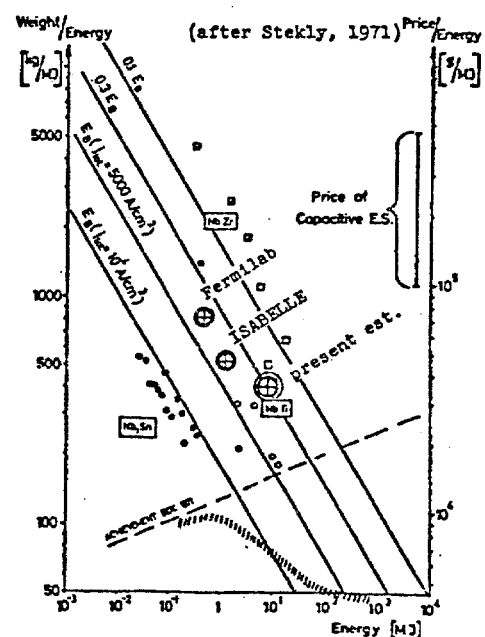
<u>Refrigerators</u> (3 x 165)	500
<u>Power supplies</u> incl. controls	500
<u>Iron shield</u> 60 m long, 3.8 m <sup>2</sup> cross section 1800 t (\$ 700/t)	1250
<u>Total magnet system:</u>	
superconducting coils, (10 6 m units)	3000
refrigerators & power supplies	1000
Iron shield	1250
	<hr/>
	<u>5250</u> =====

General remarks about cost

In fig. 10 is a comparison of prices of various coils (from 1973) illustrating the general dependency of price on magnetic stored energy. The entries for the FNAL doubler and for ISABELLE dipoles represent recent prices for single units;

presumably these prices do not include any development costs. Both these coils have a similar geometry to our 6 m unit. In our case, considering the learning costs and benefits, the first unit would probably cost somewhat more than the above estimate, but subsequent units should be somewhat cheaper. Approximately 100 k\$ would be needed to obtain necessary experimental data, especially concerning heat transport within the windings.

FIG. 10



Price & Weight per unit energy of some coils as a function of Energy. Round symbols: cylindrical coils; squares: non-rotation-symmetric.  
(from: S. L. Wipf, "Superconductive Energy Storage")  
NASA TR F-15, 109, 1973

## REFERENCES

1. S. L. Wipf, "Stability and Degradation of Superconducting Current-Carrying Devices", LASL report LA-7275, Dec 1978.
2. S. L. Wipf, "Stability of the Superconductive Operating Mode in High Current-Density Devices", IEEE Trans MAG-15, (1979), 379 - 382
3. M. A. Green, "Large Diameter Thin Superconducting Solenoid Magnets", Cryogenics, 17 (1977), 17
4. G. Vecsey, "Supercritically Cooled Muon Channel", Proc. 4th Int. Cryog. Conf, Eindhoven, 1972, p.230-32

TABLES OF DATA ( for 6m unit, unless specified otherwise)

ELECTRICAL :

Magnetic field	2 T
homogeneity over 0.8 x 0.8 m cross section	$\leq 1 \%$
operating current	2 kA
turns	796
inductance	4.32 H
stored magnetic energy	8.64 MJ
ramp time 0 - 2 T	$\geq 80$ s
voltage, for fastest ramp rate	110 V
total, all 10 units in series	1.1 kV
eddy current loss for 80 s ramp time (est.)	5 kJ
Conductor cross section 5.7 x 5.7 mm	0.325 cm <sup>2</sup>
av. conductor current density	6.15 kA/cm <sup>2</sup>
copper : superconductor ratio	16
Superconducting wires in conductor	16
diameter of wires	0.635 mm
number of NbTi filaments	360
diameter of filaments	20 $\mu$ m
twist pitch	2 cm
copper : superconductor ratio	1.8
short sample critical current density ( 2 T)	6 kA
critical current density in filaments (2T)	$3.3 \times 10^5$ A/cm <sup>2</sup>
insulation : 1 mil Kapton wrap	
overall cross section of winding, incl. pressure plates	812 cm <sup>2</sup>
overall current density	2 kA/cm <sup>2</sup>
Stability (calculated)	
full stability ( MPZ = $\infty$ ) up to	2.16 kA
(global stability, up to	1.68 kA )
Quench current (est.)	$> 2.5$ kA
Refrigerator power consumption (approx.)	
dc operation (no eddy current losses)	65 kW
maintaining 4K (cryostat losses only)	38 kW

## THERMAL

Operating temperature	4 K
heat leak at 4 K	
cryostat walls	6 W
force supports	5 W
heat leak at 70 K	
cryostat walls	80 W
force supports	30 W
Refrigerators	
two with capacity at 4 K, each	100 W
one with capacity at 70 K	1800 W
coolant:two-phase helium	
cooling circuits for each 4 K refrigerator	4
in parallel for cool-down	
in series for 4 K operation	
length of cooling circuit (all 10 units)	82.5 m
flow cross section for each circuit approx.	7 cm <sup>2</sup>
minimum coolant flow, total	6 g/s
flow speed	
as liquid	7 cm/s
as gas	50 cm/s
pressure drop (4 K operation) est.	300 Pa
helium inventory	23 l
thermal contraction, RT to 4K	2 cm
cool-down time (using no additional refrigerators) est.	7 days
superinsulation (aluminized mylar)	20 layers/cm

## MECHANICAL

Magnetic forces	
each tension strut	0.16 MN
(yield strength 0.32 MN, reached at 2.83T)	
warm supports, each 36 cm section	0.32 MN
(ultimate strength 0.5 MN, at 2.5 T)	
Weights	
cold mass	6200 kg
outer vacuum shell	2600 kg
iron shielding	1480 tons